

cMyBPC phosphorylation modulates the effect of omecamtiv mecarbil on myocardial force generation

Ranganath Mamidi*, Joshua B. Holmes*, Chang Yoon Doh, Katherine L. Dominic, Nikhil Madugula, and Julian E. Stelzer

Omecamtiv mecarbil (OM), a direct myosin motor activator, is currently being tested as a therapeutic replacement for conventional inotropes in heart failure (HF) patients. It is known that HF patients exhibit dysregulated β -adrenergic signaling and decreased cardiac myosin-binding protein C (cMyBPC) phosphorylation, a critical modulator of myocardial force generation. However, the functional effects of OM in conditions of altered cMyBPC phosphorylation have not been established. Here, we tested the effects of OM on force generation and cross-bridge (XB) kinetics using murine myocardial preparations isolated from wild-type (WT) hearts and from hearts expressing \$273A, \$282A, and \$302A substitutions (\$A) in the M domain, between the C1 and C2 domains of cMyBPC, which cannot be phosphorylated. At submaximal Ca²⁺ activations, OM-mediated force enhancements were less pronounced in \$A\$ than in WT myocardial preparations. Additionally, \$A\$ myocardial preparations lacked the dose-dependent increases in force that were observed in WT myocardial preparations. Following OM incubation, the basal differences in the rate of XB detachment (k_{rel}) between WT and \$A\$ myocardial preparations were abolished, suggesting that OM differentially affects the XB behavior when cMyBPC phosphorylation is reduced. Similarly, in myocardial preparations pretreated with protein kinase A to phosphorylate cMyBPC, incubation with OM significantly slowed k_{rel} in both the WT and \$A\$ myocardial preparations. Collectively, our data suggest there is a strong interplay between the effects of OM and XB behavior, such that it effectively uncouples the sarcomere from cMyBPC phosphorylation levels. Our findings imply that OM may significantly alter the in vivo cardiac response to β -adrenergic stimulation.

Introduction

Omecamtiv mecarbil (OM) is an inotropic agent in late-phase clinical trials that is proposed to be a general treatment for heart failure (HF) with reduced ejection fraction (EF [HFrEF]; Malik et al., 2011; Teerlink et al., 2020a). Conventional inotropic agents targeting Ca^{2+} handling, β -adrenergic signaling, or other signaling pathways have typically failed to pass clinical trials due to altered myocardial energetics, altered Ca2+ homeostasis, and an increased risk of fatal arrhythmias (Ahmad et al., 2019; Psotka et al., 2019; Holmes et al., 2020). In theory, OM avoids these issues by selectively activating myosin within cardiac sarcomeres. At the molecular level, initial preclinical studies report that OM stabilizes the force-producing state of the actin-myosin complex by increasing the rate of inorganic phosphate release from myosin (Malik et al., 2011). Other studies further revealed that OM may additionally slow the release of ADP to achieve the same effect (Liu et al., 2015; Mamidi et al., 2015). Both mechanisms serve to increase the population of strongly bound crossbridges (XBs) and to potentially counteract the decreased contractility typically seen in HFrEF. Other preclinical studies

suggest that these molecular augmentations serve to increase systolic ejection time, stroke volume (SV), and EF (Shen et al., 2010; Malik et al., 2011). HFrEF patients participating in phase 1 and 2 clinical trials largely tolerated OM while reflecting the increases in systolic ejection time, SV, and EF shown in the preclinical tests (Teerlink et al., 2020b). The general efficacy of OM is expected to be revealed by the just completed GALACTIC-HF phase 3 clinical trial with >8,000 end-stage HFrEF participants across the globe, as well as other future trials (Teerlink et al., 2020a).

Despite several high-profile clinical trials, numerous aspects of how OM interacts with the dysregulated cellular pathophysiology of HF remain poorly understood. In particular, there is a down-regulation of the PKA-mediated β -adrenergic signaling pathway that plays a critical role in the pathogenesis of HF (Lohse et al., 2003). Studies on myocardial samples from endstage failing human hearts show that sarcomeric PKA phosphorylation targets including titin, cardiac troponin I (cTnI), and cardiac myosin-binding protein C (cMyBPC) display drastically

Department of Physiology and Biophysics, School of Medicine, Case Western Reserve University, Cleveland, OH.

*R. Mamidi and J.B. Holmes contributed equally to this paper; Correspondence to Julian E. Stelzer: julian.stelzer@case.edu

This work is part of a special collection on myofilament function and disease.

© 2021 Mamidi et al. This article is distributed under the terms of an Attribution–Noncommercial–Share Alike–No Mirror Sites license for the first six months after the publication date (see http://www.rupress.org/terms/). After six months it is available under a Creative Commons License (Attribution–Noncommercial–Share Alike 4.0 International license, as described at https://creativecommons.org/licenses/by-nc-sa/4.0/).





reduced phosphorylation compared with tissue from human donor hearts (van der Velden and Stienen, 2019). Our previous study of OM in skinned human HF and donor cardiac muscle preparations suggests that the phosphorylation state of the downstream PKA targets within the sarcomere may alter the drug's effect (Mamidi et al., 2017b). However, the precise mechanisms of OM-mediated effects on down-regulated myofilament protein phosphorylation have not been rigorously examined. Thus, further characterization of the relationship between PKA phosphorylation and OM drug effects will be important to understand how OM behaves in patient populations with depressed myofilament protein phosphorylation. Other factors such as coadministered cardiovascular drugs and physiological stress such as exercise may also dynamically change phosphorylation levels within the same HFrEF patients (Wang and Fitts, 2020; Leosco et al., 2007).

Of the several sarcomeric proteins that PKA phosphorylates, cMyBPC is known to interact directly with myosin, which is OM's target (Gruen and Gautel, 1999; Moss et al., 2015; Mamidi et al., 2017a). cMyBPC is a myosin accessory protein that localizes in 9-11 bands on each side of the sarcomere's M line, anchoring to the thick filament (Craig et al., 2014). The length afforded by cMyBPC's 11 domains (CO-C10) allow its N-terminal domains to interact directly with both myosin and actin-binding sites (reviewed in Moss et al., 2015). cMyBPC's M domain between C1 and C2 harbors three physiologically important PKAphosphorylatable serine residues: S273, S282, and S302 (Tong et al., 2008; Gresham et al., 2014; Mamidi et al., 2017a). Functional studies have demonstrated that phosphorylation of these three cMyBPC residues is the principal mediator of the contractile response to increased β -adrenergic stimulation in vivo as opposed to other PKA targets (Gresham and Stelzer, 2016). Additional in vitro studies of cMyBPC phosphorylation have shown that PKA phosphorylation of cMyBPC can modulate myosin XB behavior and ATPase rate (Stelzer et al., 2007; Tong et al., 2008; Coulton and Stelzer, 2012; Mamidi et al., 2016). Collectively, these previous findings suggest that the phosphorylation state of cMyBPC may be a key modulator of OM's functional effects. Understanding the nature of the relationship between cMyBPC phosphorylation and OM will further elucidate how OM interacts with the broader pathophysiology of HFrEF.

Materials and methods

Animal protocols

Experiments conducted for this study were performed as outlined in the Guide for the Care and Use of Laboratory Animals (NIH publication no. 85-23, revised in 1996) and were conducted as per the guidelines outlined by the Institutional Animal Care and Use Committee at the Case Western Reserve University. Male and female WT and transgenic mice expressing non-phosphorylatable cMyBPC containing serine to alanine substitutions at residues S273, S282, and S302 (i.e., SA) on a cMyBPC-null background (Tong et al., 2008; Gresham and Stelzer, 2016; Mamidi et al., 2016, 2017a), aged 3-6 mo (SV/129 strain), were used for the experiments.

Relative PKA-mediated phosphorylation of cMyBPC and other sarcomeric proteins in WT and SA myocardial samples

The phosphorylation status of various myofilament proteins was assessed by phosphoprotein gel stain and Coomassie blue stain as described previously (Mamidi et al., 2014; Doh et al., 2019). Myocardial protein samples were prepared from flash-frozen mouse hearts that were stored at -80°C. Small sections of frozen ventricular tissues were thawed and homogenized in a relax buffer and incubated in 1% Triton X-100 at room temperature (\sim 23 ± 1°C) for 15 min to yield myofibrils (Mamidi et al., 2017b). After centrifugation of the samples at 10,000 rcf (relative centrifugal force) for 5 min, the pellet containing the myofibril fraction was reconstituted in relax buffer (in mM: 100 KCl, 20 imidazole, 7 MgCl₂, 2 EGTA, and 4.6 ATP, pH 7.0) containing protease and phosphatase inhibitors (PhosSTOP and cOmpleteULTRA Tablets; Sigma-Aldrich). Protein concentrations were estimated using the BCA protein colorimetric assay (Pierce BCA Protein Assay Kit; Thermo Fisher Scientific). All solutions were brought to room temperature for 10 min before initiating the PKA phosphorylation reactions. Myofibrils isolated from WT and SA hearts (100 µg) were incubated with the catalytic subunit of bovine PKA (Sigma-Aldrich) to a final concentration of 0.15 U PKA/µg myofibrils for 1 h at 30°C (Gresham et al., 2014). Control myofibrils were incubated under the same conditions without PKA. Laemmli buffer (3×) was added to stop the reaction. Samples were heated at 90°C for 10 min and stored at -20°C for future use.

For SDS PAGE, \sim 5 µg of solubilized myofibrils was loaded and separated using TruPAGE precast 4–12% gels (Sigma-Aldrich) at 180 V for 45 min. Gels were stained with Phos-Tag phosphoprotein gel stain (ABP Biosciences) using the manufacturer's instructions and imaged using the GE Healthcare Typhoon Trio Variable Mode Imager System. For total protein level determination, the gels were double stained with Blue Silver colloidal Coomassie formulation overnight and destained with water (Candiano et al., 2004). The Coomassie gels were imaged using the Azure Biosystems c600 Imaging system. Densitometric scanning of the gel images was performed using ImageJ software. The relative phosphorylation level for each protein was determined by the phosphostain intensity normalized to the Coomassie stain intensity.

Chemically skinned myocardial preparations and Ca²⁺ solutions for stretch activation experiments

Myocardial preparations were made as described previously (Gresham et al., 2014; Li et al., 2020). Flash-frozen murine ventricular tissue was homogenized in a relaxing solution and chemically skinned for 1 h with 1% Triton X-100 (Thermo Fisher Scientific). Myocardial preparations with dimensions of ~100 μ m in width and ~300 μ m in length were selected for the experiments. The composition of various Ca²⁺ activation solutions prepared for mechanical experiments was calculated using a computer program (Fabiato, 1988) and using the established stability constants (Godt and Lindley, 1982). All the Ca²⁺ solutions contained the following (in mM): 14.5 creatine phosphate, 7 EGTA, and 20 imidazole. The maximal activating solution (pCa 4.5; pCa = $-\log$ [Ca²⁺]_{free}) also contained 65.45 KCl, 7.01 CaCl₂, 5.27 MgCl₂, and 4.81 ATP, while the relaxing solution (pCa 9.0) contained 72.45 KCl, 0.02 CaCl₂, 5.42 MgCl₂, and 4.76 ATP. The



pH of the Ca²+ solutions was set to 7.0, and the ionic strength was set to 180 mM. A range of pCa solutions (pCa 6.4 to 5.5) containing varying levels of $[\text{Ca}^{2+}]_{\text{free}}$ were then prepared by mixing appropriate volumes of pCa 9.0 and pCa 4.5 stock solutions, and all the mechanical experiments were performed at ~23 ± 1°C.

Preparation of OM solution

OM was procured from Selleckchem and was dissolved in DMSO as done in our previous studies (Mamidi et al., 2015, 2017b). OM stock solution was added to a relax solution to achieve final concentrations of 0.5 μ M or 1.0 μ M OM. The final concentration of DMSO in the relax solution is 0.002%, which has negligible effects on cardiac contractile function (Takahashi et al., 2000). Incubation of the myocardial preparations with OM was done in a relax solution containing either 0.5 μ M or 1.0 μ M OM. Steady-state force generation and dynamic XB behavior were measured in myocardial preparations that were exposed to a range of pCa solutions before OM incubation, or following a 2-min incubation with either 0.5 μ M or 1.0 μ M OM (Mamidi et al., 2017b).

Apparatus for measuring steady-state and dynamic contractile properties in the myocardial preparations

Myocardial preparations were mounted between a motor arm (312C; Aurora Scientific) and a force transducer (403A; Aurora Scientific) as described previously (Li et al., 2018, 2020). Changes in the motor length and signals from the force transducer were sampled at 2,000 Hz using a custom-made sarcomere length (SL) control software program (Campbell and Moss, 2003). For all mechanical measurements, the SL of the myocardial preparations was set to 2.1 µm. Force-pCa relationships were estimated by bathing the myocardial preparations in a range of pCa solutions (i.e., pCa 6.4 to 4.5). The apparent cooperativity of force development was estimated from the steepness of Hill plot transformation of the force-pCa relationships (Mamidi et al., 2014; Chandra et al., 2009). The force-pCa data were fitted using the equation $P/P_0 = \left[\text{Ca}^{2+} \right]^{n_H} / \left(k^{n_H} + \left[\text{Ca}^{2+} \right]^{n_H} \right)$, where P is the force generated at a given pCa, P_0 is the force generated at maximal Ca^{2+} activation, n_H is the Hill coefficient, and k is the pCa required to produce half-maximal activation (i.e., pCa₅₀; Mamidi et al., 2015).

Stretch activation experiments on myocardial preparations to determine dynamic XB contractile parameters

Stretch activation experiments were performed as described in earlier publications (Li et al., 2020; Doh et al., 2019). Myocardial preparations were bathed in Ca^{2+} solutions yielding steady-state forces of ~30% of maximal Ca^{2+} -activated force. Once the myocardial preparations attained steady-state force development, a rapid 2% stretch of their initial muscle length (ML) was applied, and the preparation was held at the new ML for 8 s before being returned to the initial ML. The high-speed stretches (completed in ~2 ms) were imposed so as to minimize the changes in XB populations during the time of the imposed stretch in ML, such that the stretch activation response can be attributed to the elastic properties of the XBs that were bound to actin before the stretch (Stelzer et al., 2006b). The characteristic features of the stretch activation responses (tension transients) in cardiac

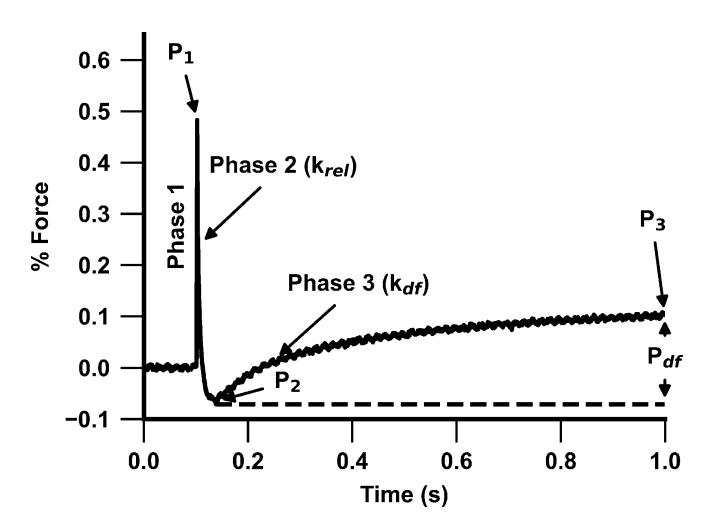


Figure 1. Representative stretch activation response following a rapid 2% stretch in ML. Highlighted are the important phases of the force response and the associated dynamic XB parameters in a WT myocardial preparation following a 2% stretch in ML (see Materials and methods for details). Phase 1 represents the immediate increase in force when a sudden stretch in ML is applied and represents the number of strongly bound XBs at the instance of the imposed stretch. P1 is the magnitude of the immediate force response and is measured from the prestretch isometric steady-state force (set to zero before the stretch) to the peak of phase 1. This is followed by phase 2, which represents a rapid decline in force development with a dynamic rate constant k_{rel} and is an index of the rate of XB detachment. The minimum point of phase 2 is represented by P2, which indicates the magnitude of XB detachment. Phase 3 denotes the delayed force development with a dynamic rate constant $k_{\rm df}$ and is an index of the rate of XB recruitment. P_{df} is the difference between P2 and P3 and represents the magnitude of XB recruitment in response to the imposed stretch.

muscle have been described in detail elsewhere (Stelzer and Moss, 2006; Ford et al., 2010; Mamidi et al., 2019) and are shown in Fig. 1. Various phases of the tension transients elicited in response to ML changes were then analyzed individually to gain insights into XB mechanics (Stelzer et al., 2006a; 2006b; 2006c; 2007).

A sudden 2% stretch of ML induces an instantaneous rise in force (P1), which is due to the strain of strongly bound XBs (phase 1) and represents the number of strongly bound XBs in a force-producing state (XB stiffness; Stelzer and Moss, 2006; Ford et al., 2010). The force transient then rapidly decays (phase 2) due to a rapid detachment of the strained XBs, which transition into a non-force-generating state, with a rate constant $k_{\rm rel}$, an index of XB detachment from actin. The minimum force reached at the end of phase 2 of the stretch activation transient is indicated by P2 and represents the magnitude of XB detachment following stretch. The amplitude of P2 can decline further than the isometric prestretch force, resulting in negative values, especially following PKA treatment, which is likely due to an acceleration in the rate of XB detachment in phase 2 (Stelzer et al., 2006c). Following phase 2 is a gradual rise in force development (phase 3), with a rate constant k_{df} , which is a result of stretchinduced recruitment of additional XBs into the force-generating state, and the amplitude of phase 3 is an index of the magnitude of XB recruitment (P_{df}). The new peak of the steady-state force, which is higher than the initial prestretch steady-state force,



attained in response to the increase in ML is indicated by P3. The sum of all XBs recruited by a sudden 2% stretch in ML in an isometrically contracting myocardial preparation can be assessed by measuring the amplitude of the delayed force response of phase 3 (i.e., $P_{\rm df}$).

The different stretch activation amplitudes were normalized to prestretch Ca^{2+} -activated force to facilitate comparisons between preparations that develop different amounts of absolute force and the Ca^{2+} activation levels as done before (Mamidi et al., 2015, 2018, 2017b). Thus, the amplitudes of all parameters measured are expressed as a fraction of the total prestretch forces (Mamidi et al., 2017b). P1 is measured from the prestretch steady-state force to the peak of phase 1; P2 is measured from the prestretch steady-state force to the minimum force value attained at the end of phase 2; P3 is measured from the prestretch steady-state force to the peak force value of the delayed force attained in phase 3; and $P_{\rm df}$ is the difference between P3 and P2.

 $k_{\rm rel}$ was measured by fitting a single exponential to the time course of force decay using the formula $y=a[-1+\exp(-k_1\times x)]$, where a is the amplitude of the single exponential phase and k_1 is the rate constant of the force decay (Mamidi et al., 2016). $k_{\rm df}$ was estimated by linear transformation of the half-time of force redevelopment ($k_{\rm df}=0.693/t_{1/2}$), where $t_{1/2}$ is the time in milliseconds measured from the nadir (i.e., the point of force reuptake at the end of phase 2) to achievement of the half-maximal force in phase 3 of the force response, where maximal force is indicated by the achievement of a plateau region in phase 3 (P3; Mamidi et al., 2016).

Stretch activation experiments were performed following a 1-h incubation of the myocardial preparations with PKA. Because PKA treatment decreases the myofilament Ca^{2+} sensitivity of force generation, we used a pCa solution with slightly higher $[Ca^{2+}]_{\rm free}$ (pCa 6.0) to match the activation levels before PKA treatment (pCa 6.1; Mamidi et al., 2016).

Data analysis

All data are presented as mean \pm SEM. Data from multiple myocardial preparations from each heart were averaged to provide a single value that was then used for the statistical analysis. Multiple groups of data were analyzed using a two-way ANOVA followed by Tukey post-hoc tests. The type of myocardial preparation (WT or SA) and the dose of OM (pre-OM [0.0 μ M OM], 0.5 μ M OM, or 1.0 μ M OM) were the two factors for the analysis. Wherever appropriate, independent t tests were used to assess whether there were any significant differences between two different groups, and pairwise t tests were used to assess whether there were any significant differences before and after OM incubations on the same myocardial preparation as in our previous studies (Mamidi et al., 2015, 2017b). The criterion for statistical significance was set at P < 0.05.

Results

Impact of cMyBPC phosphoablation on sarcomeric protein isoform phosphorylation

We have previously demonstrated that the expression of cMyBPC in SA hearts is \sim 73 \pm 8% of WT cMyBPC levels

(Gresham and Stelzer, 2016; Mamidi et al., 2016) and that M domain phosphorylation (i.e., S273, S282, and S302) is abolished (Gresham and Stelzer, 2016; Mamidi et al., 2016). These SA mice have been characterized in our earlier studies (Mamidi et al., 2016, 2017a), and the expression level of the transgenic SA reported in this study is comparable to that of other published studies (Tong et al., 2008; Rosas et al., 2015). We have also previously shown that OM treatment does not alter the phosphorylation status of sarcomeric proteins (Mamidi et al., 2015). The phosphorylation levels of sarcomeric proteins in cardiac samples prepared from WT and SA hearts were analyzed by SDS gel electrophoresis and Phos-Tag phosphoprotein gel stain analysis (Fig. 2 A). To assess the impact of cMyBPC phosphoablation on PKA-mediated phosphorylation of myofilament proteins, WT and SA samples were incubated with PKA for 1 h at 30°C (Mamidi et al., 2016). As expected, the phosphorylation of cMyBPC increased following the PKA treatment in the WT samples (Fig. 2 B). Interestingly, the cMyBPC phosphorylation level in SA samples also increased modestly following PKA treatment but did not reach the WT levels (Fig. 2 B). This modest increase is likely due to the phosphorylation of other PKA sites in cMyBPC (Kooij et al., 2013; Bardswell et al., 2012). However, as we and others have previously shown (Gresham et al., 2014; Gresham and Stelzer, 2016; Tong et al., 2008; Nagayama et al., 2007), these phosphorylation residues appear functionally less significant in vivo.

Effects of OM on Ca²⁺-activated force generation in WT and SA myocardial preparations

Myocardial preparations were sequentially bathed in Ca²⁺ solutions containing increasing Ca2+ levels (pCa 6.2, 6.1, 6.0, and 5.9) to yield submaximal forces (~18-40% of maximal force) as done previously (Mamidi et al., 2015). Force generation was first measured at baseline, and again following a 2-min incubation in 0.5 µM or 1.0 µM OM (Mamidi et al., 2015, 2017b). The force enhancement following OM incubation is expressed as the percent increase in force from the corresponding baseline force (considered as 100% force) generated by the myocardial preparation at a given Ca2+ activation. The OM-induced force enhancements gradually decreased as the level of Ca2+ activation increased (Table 1, Table 2, Fig. 3, and Fig. 4), as observed previously. Force generations and percent force increases following OM incubation in WT and SA myocardial preparations are shown in Table 1 and Table 2, respectively. Importantly, OMinduced force enhancement was more pronounced in the WT myocardial preparations than in SA myocardial preparations, especially with 1.0 µM OM at pCa values 6.2 and 6.1 (Table 1 and Table 2). Specifically, the percent force increases in WT myocardial preparations following 1.0 µM OM incubation at pCa values 6.2 and 6.1 were 157 \pm 15 and 63 \pm 3, respectively, whereas the percent force increases in SA myocardial preparations were only 51 \pm 8 and 33 \pm 9 (Table 2). Furthermore, no significant differences were observed between the pre-OM force development in the SA myocardial preparations when compared with the WT myocardial preparations at either submaximal Ca²⁺ activations (Table 1) or maximal Ca²⁺ activation (Table 3). Thus, the decreased force enhancements at submaximal Ca2+



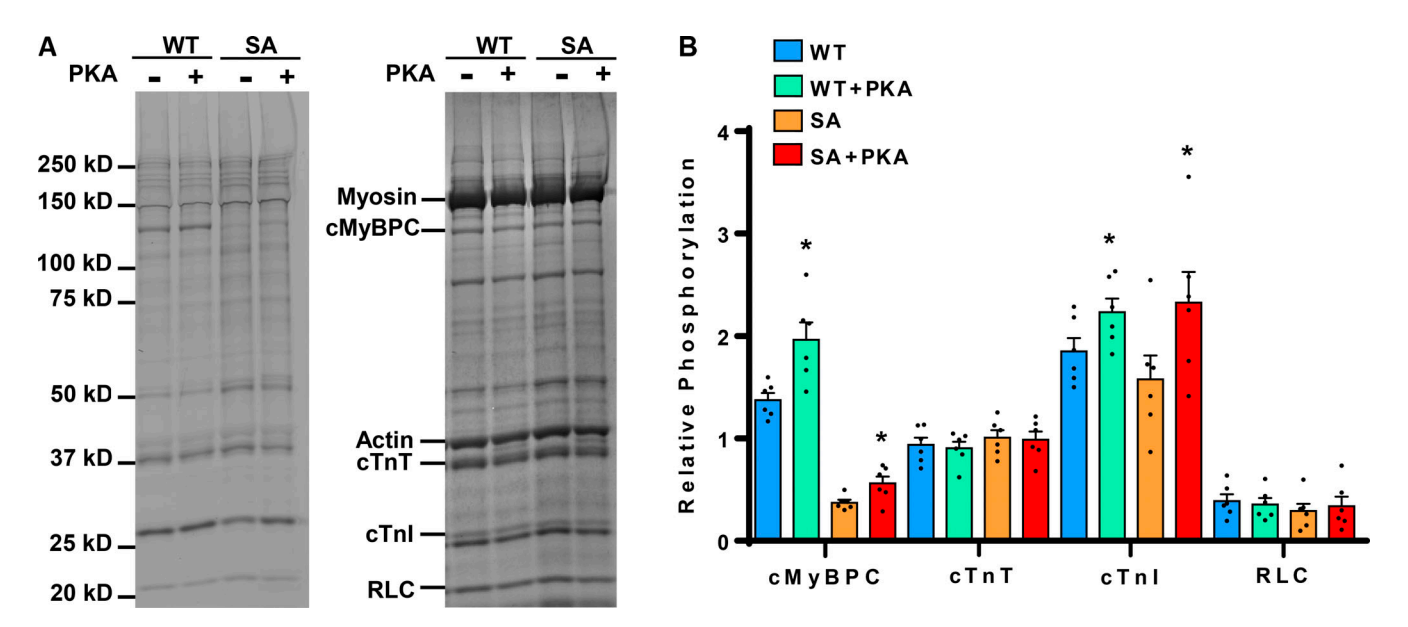


Figure 2. Phos-Tag phosphoprotein gel stain analysis to assess the phosphorylation status of myofilament proteins in WT and SA myocardial preparations. (A) Representative Phos-Tag phosphoprotein–stained (left) and Coomassie-stained (right) SDS gels showing the phosphorylation status of myofilament proteins in WT and SA samples before and following incubation with PKA. (B) Quantification of phosphorylation of cMyBPC, cTnT, cTnI, and RLC in WT and SA samples. In both groups, three hearts and two replicates each were used to analyze total protein expression and phosphorylation. Values are expressed as mean ± SEM. *, Significantly different compared with the corresponding pre-PKA group; P < 0.05.

activations following 1.0 μ M OM in the SA myocardial preparations can be attributed to cMyBPC phosphoablation in the SA myocardial preparations. Another important finding is that OM incubation led to dose-dependent increases in the myocardial force generation at all the Ca²⁺ levels tested in WT myocardial preparations but not in SA myocardial preparations (Table 2 and Fig. 3). Taken together, our data suggest that OM is not as effective at enhancing force generation in myocardial preparations with dephosphorylated cMyBPC.

We next tested whether PKA treatment, which is known to phosphorylate both cMyBPC and cTnI, alters the OM-induced effects on myocardial force generation. Because 0.5 μ M OM did not result in significant force enhancements in the SA myocardial preparations, we incubated the PKA-treated WT and SA myocardial preparations with 1.0 μ M OM. For PKA-treated WT myocardial preparations, the forces (in mN/mm²) before and after OM treatment, respectively, were, for pCa 6.2, 2.20 \pm 0.32 and 6.58 \pm 0.37; pCa 6.1, 3.31 \pm 0.33 and 6.79 \pm 0.70; pCa 6.0, 4.40 \pm

Table 1. Force generation in WT and SA myocardial preparations following OM incubations at different levels of Ca²⁺ activation

Group	pCa 6.2	pCa 6.1	pCa 6.0	pCa 5.9
WT				
Pre-0.5 μM OM	4.9 ± 0.7	8.7 ± 1.2	9.3 ± 1.2	12.4 ± 1.9
0.5 μM OM	7.7 ± 0.8 (*, P = 0.001)	10.4 ± 1.4 (*, P = 0.03)	9.8 ± 1.0	11.7 ± 1.3
Pre-1.0 μM OM	3.7 ± 0.6	6.3 ± 0.8	7.7 ± 1.2	10.2 ± 1.9
1.0 μM OM	9.3 ± 0.9 (*, P = 0.001)	10.2 ± 1.1 (*, P = 0.001)	9.5 ± 1.2 (*, P = 0.007)	11.4 ± 1.7 (*, P = 0.03)
SA				
Pre-0.5 μM OM	4.5 ± 0.9	5.3 ± 0.9	7.4 ± 1.2	9.1 ± 1.2
0.5 μM OM	4.9 ± 0.7	6.1 ± 1.4	7.3 ± 1.0	9.1 ± 1.1
Pre-1.0 μM OM	4.2 ± 0.6	5.3 ± 0.7	6.9 ± 0.5	7.8 ± 0.5
1.0 μM OM	6.3 ± 0.7 (*, P = 0.001; &, P = 0.03)	6.9 ± 0.6 (*, P = 0.008; &, P = 0.04)	8.1 ± 0.6 (*, P = 0.01)	8.7 ± 0.4 (*, P = 0.01)

The impact of OM on force generation was measured by incubating WT and SA myocardial preparations with either $0.5 \mu M$ or $1.0 \mu M$ OM. Baseline forces generated by the myocardial preparations were first measured in Ca^{2+} solutions with a range of pCa values from 6.2 to 5.9. Forces (in mN/mm²) were subsequently measured on the same preparations using the same range of pCa solutions following a 2-min incubation with either $0.5 \mu M$ or $1.0 \mu M$ OM. Data from multiple preparations from each heart were averaged, and 12-15 myocardial preparations from four different hearts were used per group. Values are expressed as mean \pm SEM. *, Significantly different when comparing the forces generated prior to OM incubation with forces generated following OM incubation within each group. &, Significantly different compared with the corresponding WT group.

Variable cMyBPC phosphorylation and OM response



Table 2. Percentage changes in force generation in WT and SA myocardial preparations following OM incubations at different levels of Ca²⁺ activation

Group	pCa 6.2	pCa 6.1	pCa 6.0	pCa 5.9
WT				
0.5 μM OM	62.3 ± 8.7 (*, P = 0.006)	19.4 ± 4.0 (*, P = 0.02)	6.44 ± 3.1	-3.7 ± 4.3
1.0 μM OM	157.4 ± 15.1 (*, P = 0.002; #, P = 0.001)	62.7 ± 3.2 (*, P = 0.0003; *, P = 0.003)	25.6 ± 5.2 (*, P = 0.02; #, P = 0.02)	14.4 ± 4.4 (*, P = 0.04; #, P = 0.02)
SA				
0.5 μM OM	16.7 ± 16.2	10.3 ± 8.6	0.8 ± 4.2	-0.02 ± 3.3
1.0 μM OM	51.3 ± 7.9 (*, P = 0.007; &, P = 0.0003)	32.5 ± 8.7 (*, P = 0.03; &, P = 0.03)	15.4 ± 2.5 (*, P = 0.01)	11.1 ± 2.4 (*, P = 0.02)

The impact of OM on force generation was measured by incubating WT and SA myocardial preparations with either $0.5~\mu M$ or $1.0~\mu M$ OM. Baseline forces generated by the myocardial preparations were first measured in Ca²⁺ solutions with a range of pCa values from 6.2 to 5.9. Forces were subsequently measured on the same preparations using the same range of pCa solutions following a 2-min incubation with either $0.5~\mu M$ or $1.0~\mu M$ OM. The net increase in force generation following OM incubation at each pCa was calculated and expressed as percent increase in force from the baseline as done previously (Mamidi et al., 2015, 2017b). Data from multiple preparations from each heart were averaged, and 12-15 myocardial preparations from four different hearts were used per group. Values are expressed as mean \pm SEM. #, Significantly different compared to the $0.5~\mu M$ OM group. *, Significantly different comparing baseline forces to the forces generated following incubation with OM within each group. &, Significantly different compared to the corresponding WT group.

1.08 and 6.42 \pm 1.08; and pCa 5.9, 6.82 \pm 0.78 and 7.73 \pm 0.61. For PKA-treated WT myocardial preparations, the percent force increases from baseline were 215.4 \pm 53.2, 105.1 \pm 8.9, 54.6 \pm 17.8, and 14.5 ± 5.8, respectively, at pCa 6.2, 6.1., 6.0, and 5.9. For PKAtreated SA myocardial preparations, the forces (in mN/mm²) before and after OM treatment, respectively, were, for pCa 6.2, 3.46 \pm 0.89 and 5.16 \pm 1.41; pCa 6.1, 3.43 \pm 0.67 and 5.39 \pm 1.09; pCa 6.0, 4.13 ± 0.77 and 5.71 ± 1.10 ; and pCa 5.9, 5.24 ± 1.15 and 6.32 ± 1.36 . For PKA-treated SA myocardial preparations, the percent force increases from baseline were 49.5 \pm 7.9, 57.5 \pm 5.7, 37.8 \pm 1.1, and 21.1 ± 5.4, respectively, at pCa 6.2, 6.1., 6.0, and 5.9. Similar to the non-PKA-treated myocardial preparations, the percent force increases in the SA myocardium were significantly smaller when compared with force increases in the WT myocardial preparations, especially at low Ca²⁺ activations (pCa 6.2 and 6.1). Thus, our results show that cMyBPC phosphorylation modulates the impact of OM on force generation. Incubation with OM did not alter the maximal Ca²⁺-activated force (i.e., Fmax measured at pCa 4.5) or the Ca²⁺-independent force (i.e., Fmin measured at pCa 9.0; Table 3 and Table 4).

Effects of OM on myofilament Ca^{2+} sensitivity (pCa₅₀) of force generation and cooperativity (n_H) in WT and SA myocardial preparations

The effect of OM on pCa₅₀, the pCa required to generate half-maximal force, was assessed by plotting normalized force values against a range of pCa and constructing force-pCa relationships at SL 2.1 μ m in WT and SA myocardial preparations. The pCa₅₀ was estimated by fitting the Hill equation to the force-pCa relationships (Fig. 5). The pCa₅₀ values for WT and SA myocardial preparations before and following OM treatment in non-PKA-treated groups and PKA-treated groups are shown in Table 3 and Table 4, respectively. Our data show that treatment with both 0.5 μ M and 1.0 μ M OM increased the responsiveness of the

cardiac myofilaments to Ca^{2+} at submaximal Ca^{2+} activations in the WT myocardial preparations, as indicated by a significant leftward shift in the force–pCa relationships in all the groups (Fig. 5 A and Table 3). The $n_{\rm H}$ values decreased after OM treatment in the WT myocardial preparations, indicating that incubation with OM decreased the overall cooperativity of force generation (Mamidi et al., 2015; Table 3). In contrast to WT myocardial preparations, pCa₅₀ was unaltered in the SA myocardial preparations following OM incubations, presumably because no significant force enhancements occurred following 0.5 μ M OM incubation and that 1.0 μ M OM-mediated force enhancements were mainly confined to <50% of maximal force (P = 0.07). As a result, $n_{\rm H}$ values decreased only after 1.0 μ M OM treatment in the SA myocardial preparations (Table 3).

Incubation with 1.0 μ M OM did not significantly increase the pCa₅₀ in PKA-treated myocardial preparations, likely because most of the OM-mediated force enhancements are confined to <50% of maximal force. Furthermore, treatment with 1.0 μ M OM decreased the $n_{\rm H}$ in PKA-treated WT myocardial preparations (Table 4).

Effects of OM on dynamic stretch activation parameters in WT and SA myocardial preparations

Stretch activation parameters (Fig. 1) were assessed following OM incubations (0.5 μ M or 1.0 μ M) at pCa 6.1 in WT and SA myocardial preparations (Table 5). Pre- and post-OM stretch activation traces shown for non-PKA-treated (Fig. 6) and PKA-treated (Fig. 7) myocardial preparations were collected at pCa values 6.1 and 6.0, respectively. The impact of OM on the rate of XB detachment was assessed by measuring $k_{\rm rel}$. We have previously shown that 1.0 μ M OM slows $k_{\rm rel}$ in murine myocardial preparations (Mamidi et al., 2015). As shown previously (Mamidi et al., 2016, 2017a), under basal conditions (before OM treatment) SA myocardial preparations exhibited a slower $k_{\rm rel}$



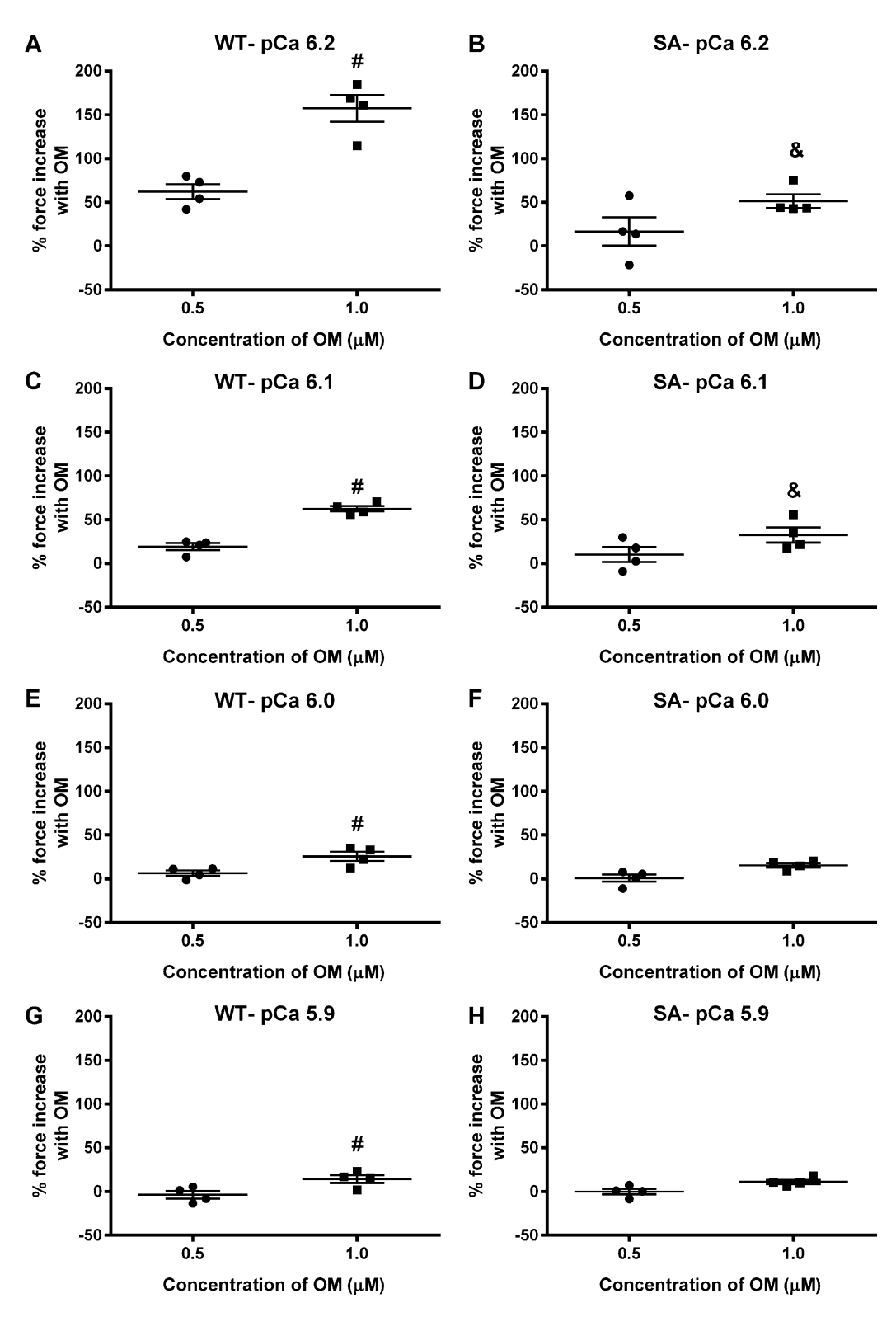


Figure 3. Impact of OM on percent force increases at various levels of Ca^{2+} activation in WT and SA myocardial preparations. (A–H) Baseline forces generated by the myocardial preparations were initially measured in Ca^{2+} solutions with pCa ranging from 6.2 to 5.9. Forces were subsequently measured on the same preparations using the same range of pCa solutions following a 2-min incubation with either 0.5 or 1.0 μ M OM. The net increase in force generation following OM incubation at each pCa was calculated and expressed as percent increase in force from the preincubation baseline force in WT and SA myocardial preparations as done in our previous studies (Mamidi et al., 2015, 2017b). Incubation with OM led to a dose-dependent increase in the myocardial force generation at all the Ca^{2+} levels tested in the WT but such dose-dependent force increases were absent in the SA myocardial preparations. Data from multiple preparations from each heart were averaged, and 12–15 myocardial preparations from four different hearts were used per group. Values are expressed as mean \pm SEM. #, Significantly different compared with the corresponding WT group. P < 0.05.



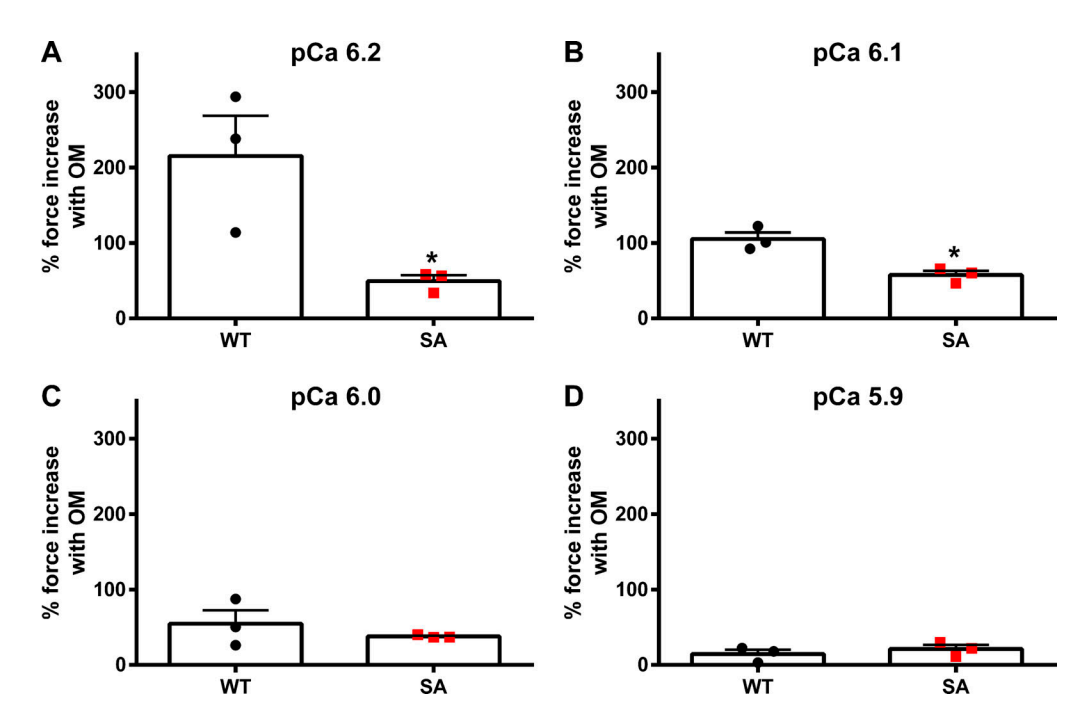


Figure 4. Impact of OM on the magnitude of force generation at various levels of Ca^{2+} activation in PKA-treated WT and SA myocardial preparations. (A–D) Myocardial preparations were incubated for 1 h in PKA, and then baseline forces generated by the PKA-treated preparations were first measured in Ca^{2+} solutions with pCa ranging from 6.2 to 5.9. Forces were subsequently measured on the same myocardial preparations using the same range of pCa solutions following a 2-min incubation with 1.0 μ M OM. The net increase in force generation following OM incubation at each pCa was calculated and expressed as percent increase in force from the preincubation baseline force measured in Ca^{2+} solutions with pCa 6.2 (A), 6.1 (B), 6.0 (C), and 5.9 (D). Force enhancements following OM incubation were less pronounced in the PKA-treated SA myocardial preparations when compared with the PKA-treated WT myocardial preparations, especially at low Ca^{2+} activations, where OM has more potent effects on enhancing the force generation (Mamidi et al., 2015, 2017b). Data from multiple preparations from each heart were averaged, and six to seven myocardial preparations from three different hearts were used per group. Values are expressed as mean \pm SEM. *, Significantly different compared with the corresponding 1.0 μ M OM-treated WT group; P < 0.05.

when compared with the WT myocardial preparations. Following 0.5 μ M and 1.0 μ M OM incubation, $k_{\rm rel}$ slowed by ~50% and ~74%, respectively, in the WT myocardial preparations (Fig. 8 A). Interestingly, in the SA myocardial preparations, 0.5 μ M OM incubation did not slow $k_{\rm rel}$, but 1.0 μ M OM incubation slowed $k_{\rm rel}$ by ~72% (Fig. 8 B), indicating a differential effect of OM dose on $k_{\rm rel}$ in myocardial preparations with dephosphorylated

cMyBPC. Thus, following OM incubations, $k_{\rm rel}$ differences between WT and SA myocardial preparations were abolished.

The impact of OM on the rate of XB recruitment was assessed by measuring $k_{\rm df}$. We have previously shown that 1.0 μ M OM slows $k_{\rm df}$ in the murine myocardial preparations (Mamidi et al., 2015). Under basal conditions, no differences in $k_{\rm df}$ existed between WT and SA myocardial preparations, as shown previously

Table 3. Steady-state contractile parameters measured in WT and SA myocardial preparations

Group	pCa ₅₀	n _H	Fmax (mN/mm²)	Fmin (mN/mm²)
WT				
Pre-OM	5.85 ± 0.03	2.22 ± 0.09	18.13 ± 2.87	1.16 ± 0.21
0.5 μM OM	6.02 ± 0.01 (*, P = 0.005)	1.49 ± 0.04 (*, P = 0.0008)	13.47 ± 3.01	1.61 ± 0.31
1.0 μM OM	6.08 ± 0.04 (*, P = 0.0002)	1.03 ± 0.02 (*, P < 0.0001)	12.26 ± 1.83	1.92 ± 0.19
SA				
Pre-OM	5.86 ± 0.02	2.10 ± 0.12	12.95 ± 1.77	1.02 ± 0.24
0.5 μM OM	5.79 ± 0.03 (&, P = 0.005)	2.05 ± 0.14 (&, P = 0.01)	12.21 ± 1.29	1.70 ± 0.33
1.0 μΜ ΟΜ	5.97 ± 0.02	1.33 ± 0.02 (*, P = 0.0005)	9.10 ± 1.03	1.15 ± 0.25

pCa₅₀, myofilament Ca²⁺ sensitivity; $n_{\rm H}$, cooperativity of force production; Fmax, maximal Ca²⁺-activated force measured at pCa 4.5; Fmin, Ca²⁺-independent force measured at pCa 9.0. Values are expressed as mean \pm SEM. Data from multiple preparations from each heart were averaged, and 9–13 myocardial preparations from three or four hearts were used per group. *, Significantly different compared with the corresponding pre-OM group. &, Significantly different compared with the corresponding WT group.



Table 4. Steady-state contractile parameters measured in PKA-treated WT and SA myocardial preparations

Group	pCa ₅₀	n _H	Fmax (mN/mm²)	Fmin (mN/mm²)
WT + PKA				
Pre-OM	5.77 ± 0.03	2.04 ± 0.06	17.44 ± 1.68	0.58 ± 0.04
1.0 μM OM	5.99 ± 0.10	1.07 ± 0.07 (*, P = 0.02)	13.54 ± 0.08	1.52 ± 0.08
SA + PKA				
Pre-OM	5.79 ± 0.02	2.13 ± 0.13	14.88 ± 0.33	1.54 ± 0.21
1.0 μM OM	5.92 ± 0.08	1.52 ± 0.32	11.43 ± 2.77	2.19 ± 0.54

 pCa_{50} , myofilament Ca^{2+} sensitivity; n_H , cooperativity of force production; Fmax, maximal Ca^{2+} -activated force measured at pCa 4.5; Fmin, Ca^{2+} -independent force measured at pCa 9.0. Values are expressed as mean \pm SEM. Data from multiple preparations from each heart were averaged, and six to seven myocardial preparations from three different hearts were used per group. *, Significantly different compared with the corresponding pre-OM group.

(Mamidi et al., 2016, 2017a). In WT myocardial preparations, $k_{\rm df}$ slowed only with 1.0 μ M OM (by ~24%), but $k_{\rm df}$ was slowed with both 0.5 μ M OM (by ~29%) and 1.0 μ M OM (by ~45%) in SA myocardial preparations (Table 5 and Fig. 8, C and D).

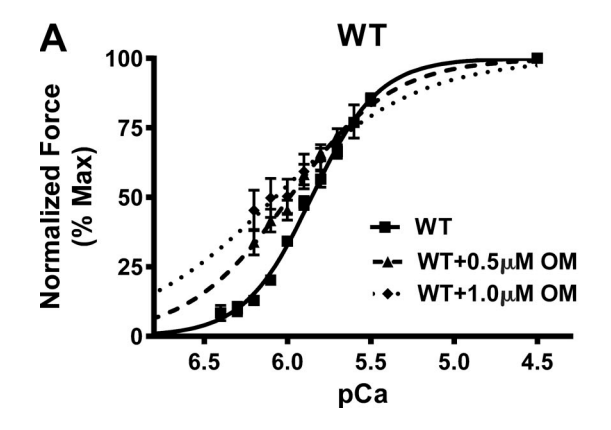
The impact of OM on the magnitude of the stiffness of strongly bound force-generating XBs was assessed by measuring P1 from the stretch activation responses in the WT and SA myocardial preparations (Fig. 1). Our data show that P1 significantly increased, by $\sim\!20\%$ and $\sim\!43\%$, following 0.5 μM and 1.0 μM OM, respectively, in WT myocardial preparations. P1 increased by $\sim\!19\%$ and $\sim\!16\%$ following 0.5 μM and 1.0 μM OM, respectively, in SA myocardial preparations. Therefore, following 1.0 μM OM incubation, P1 in SA myocardial preparations was significantly smaller when compared with the corresponding WT myocardial preparations (Table 5 and Fig. 8, E and F), indicating a blunting in the OM-induced increase in P1 in myocardial preparations with dephosphorylated cMyBPC.

The impact of OM on the magnitude of the XB detachment was assessed by measuring P2 from the stretch activation responses (Table 5 and Fig. 1). Our data show that P2 significantly increased following 0.5 μ M and 1.0 μ M OM in WT myocardial preparations. Despite not reaching statistical significance, P2

values showed an increasing trend following increased OM concentrations in the SA myocardial preparations, indicating a differential effect of OM on P2 (Table 5).

The impact of OM on the magnitude of the new steady-state force development due to ML-mediated recruitment of additional XBs was assessed by measuring P3 from the stretch activation responses in the WT and SA myocardial preparations (Table 5 and Fig. 1). Our data indicate that P3 was unaltered by OM treatment in the WT and SA myocardial preparations. This finding is in contrast to a previous report which showed ~16% increase in E_R (equivalent to P3) at maximal Ca²⁺ activation in chemically skinned guinea pig cardiac muscle preparations (Gollapudi et al., 2017). While the cause for this divergent finding is currently unknown, it may be related to the differences in the level of Ca²⁺ activation used between the two studies (pCa 6.1 in our study vs. pCa 4.3 in Gollapudi et al., 2017). However, our observations are in agreement with an unaltered E_R at submaximal Ca²⁺ activations (pCa 5.8) reported in the same study.

The impact of OM on the magnitude of XB recruitment following a sudden stretch in ML was assessed by measuring $P_{\rm df}$. As shown previously (Mamidi et al., 2016, 2017b), under basal



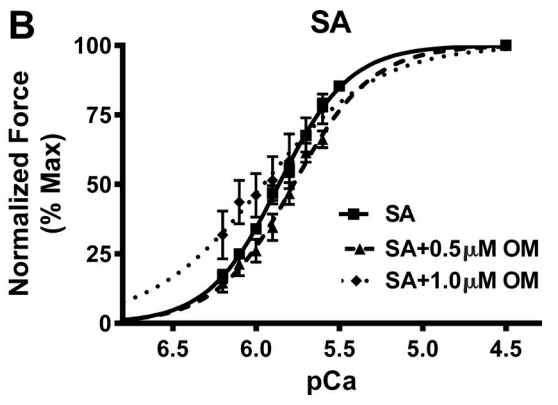


Figure 5. Impact of OM on myofilament Ca^{2+} sensitivity (pCa₅₀) in WT and SA myocardial preparations. (A and B) Force-pCa relationships were constructed by plotting normalized forces generated against a range of pCa with and without OM incubations in WT (A) and SA (B) myocardial preparations. OM incubation caused a significant leftward shift in the force-pCa relationships in WT myocardial preparations, indicating that OM caused a significant increase in pCa₅₀. However, pCa₅₀ was unaltered in the SA myocardial preparations following OM incubation, presumably because 1.0 μ M OM-mediated force enhancements in SA myocardial preparations were mainly confined to <50% of maximal force. Data from multiple preparations from each heart were averaged, and 9–13 myocardial preparations from three or four hearts were used per group.



Table 5. Dynamic stretch activation parameters measured in WT and SA myocardial preparations

Group	k _{rel} (s ⁻¹)	k _{df} (s ⁻¹)	P1	P2	Р3	P_{df}
WT						
Pre-OM	345.39 ± 16.71	4.21 ± 0.30	0.554 ± 0.02	-0.093 ± 0.01	0.165 ± 0.01	0.258 ± 0.01
0.5 μM OM	171.24 ± 14.54 (*, P < 0.0001)	3.56 ± 0.19	0.665 ± 0.01 (*, P = 0.03)	0.012 ± 0.01 (*, P = 0.02)	0.158 ± 0.01	0.146 ± 0.02 (*, P = 0.001)
1.0 μM OM	89.95 ± 14.26 (*, P < 0.0001)	3.18 ± 0.37 (*, P = 0.04)	0.792 ± 0.03 (*, P < 0.0001)	0.076 ± 0.01 (*, P < 0.0001)	0.155 ± 0.02	0.079 ± 0.01 (*, P < 0.0001)
SA						
Pre-OM	217.15 ± 23.47 (%, P = 0.001)	4.23 ± 0.09	0.561 ± 0.02	0.046 ± 0.02 (&, P = 0.001)	0.179 ± 0.01	0.133 ± 0.01 (&, P = 0.0005)
0.5 μM OM	157.48 ± 29.34	2.99 ± 0.15 (*, P = 0.02)	0.665 ± 0.02 (*, P = 0.04)	0.110 ± 0.04 (&, P = 0.03)	0.223 ± 0.02 (&, P = 0.04)	0.113 ± 0.03
1.0 μM OM	61.67 ± 8.28 (*, P = 0.0002)	2.30 ± 0.18 (*, P = 0.0002)	0.653 ± 0.02 (&, P = 0.002)	0.118 ± 0.01	0.161 ± 0.01	0.043 ± 0.01 (*, P = 0.01)

Stretch activation amplitudes were normalized to prestretch steady-state Ca^{2+} -activated force, which refers to the activation level (pCa 6.1; ~30% of maximal Ca^{2+} -activated force) as described in Materials and methods. Data from multiple preparations from each heart were averaged, and 12–15 myocardial preparations from four or five different hearts were used per group. Values are expressed as mean \pm SEM. k_{dfr} rate of XB recruitment; k_{relr} rate of XB detachment; P1, XB stiffness; P2, magnitude of XB detachment; P3, new steady-state force reached following a quick 2% stretch in ML; k_{dfr} magnitude of XB recruitment. *, Significantly different compared with the corresponding pre-OM group. &, Significantly different compared with the corresponding WT group.

conditions, SA myocardial preparations exhibited a smaller $P_{\rm df}$ compared with WT myocardial preparations (Table 5). Following 0.5 μ M and 1.0 μ M OM incubations, $P_{\rm df}$ decreased by ~43% and ~70%, respectively, in WT myocardial preparations (Fig. 8 G). In contrast, in SA myocardial preparations, incubation with 0.5 μ M OM did not alter $P_{\rm df}$, whereas incubation with 1.0 μ M OM decreased $P_{\rm df}$ by ~68% (Fig. 8 H).

Effects of OM on dynamic stretch activation parameters in PKA-treated WT and SA myocardial preparations

The effect of 1.0 μ M OM incubation on stretch activation parameters was tested at pCa 6.0 in PKA-treated WT and SA myocardial preparations (Table 6). $k_{\rm rel}$ in the PKA-treated SA myocardial preparations was slower when compared with PKA-treated WT myocardial preparations, as reported previously (Mamidi et al., 2016; Table 6). Following OM incubation, $k_{\rm rel}$ slowed by ~78% in the WT myocardial preparations, but $k_{\rm rel}$ slowed by only ~53% in the SA myocardial preparations, such that $k_{\rm rel}$ differences between PKA-treated WT and SA

myocardial preparations were abolished (Table 6 and Fig. 9, A and B). $k_{\rm df}$ in the PKA-treated SA myocardial preparations was slower than $k_{\rm df}$ in the PKA-treated WT myocardial preparations, as reported previously (Mamidi et al., 2016; Table 6). Following OM incubation, $k_{\rm df}$ slowed by ~66% in WT myocardial preparations, but $k_{\rm df}$ slowed by only ~52% in SA myocardial preparations, such that k_{df} differences between PKA-treated WT and SA myocardial preparations were abolished after OM treatment (Table 6 and Fig. 9, C and D). Furthermore, OM incubation increased the magnitude of the strongly bound XBs (P1) in PKAtreated WT and SA myocardial preparations (Fig. 9, E and F). As shown previously (Mamidi et al., 2016, 2017a), PKA-treated SA myocardial preparations exhibited a smaller magnitude of XB recruitment, P_{df} when compared with the PKA-treated WT myocardial preparations (Mamidi et al., 2016; Table 6). Incubation with OM decreased P_{df} in PKA-treated WT and SA myocardial preparations, and P_{df} in the SA myocardial preparations was reduced compared with WT myocardial preparations (Fig. 9, G and H).

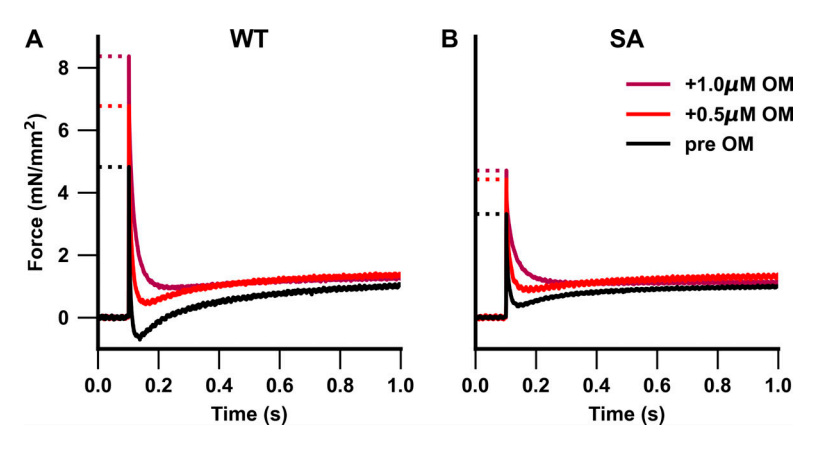


Figure 6. Representative stretch activation traces from WT and SA myocardial preparations. (A and B) Representative stretch activation responses to a rapid 2% increase in ML in WT (A) and SA (B) myocardial preparations measured at pCa 6.1 to illustrate the dose-dependent effect of OM on force generation. WT myocardial preparations showed a dose-dependent OM-mediated increase in force development, whereas increase in force development was observed only following 1.0 μM OM incubation in the SA myocardial preparations.



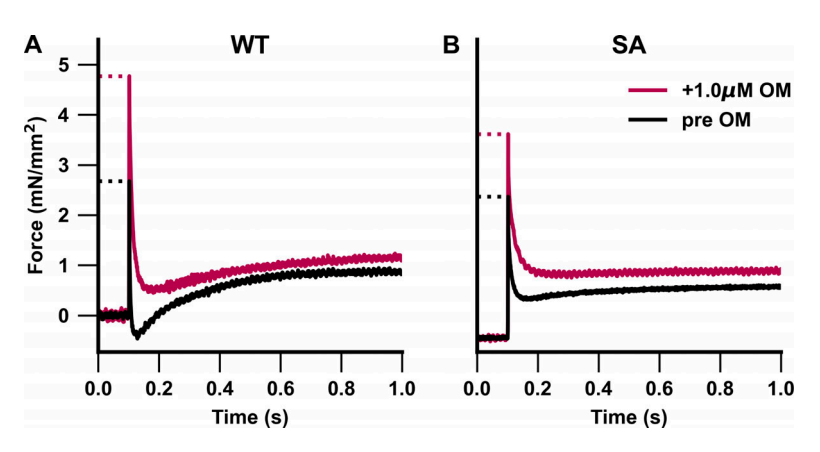


Figure 7. Representative stretch activation traces from PKA-treated WT and SA myocardial preparations. (A and B) Representative stretch activation responses to a rapid 2% increase in ML in PKA-treated WT (A) and PKA-treated SA (B) myocardial preparations measured at pCa 6.0 to illustrate the effect of OM on force generation. Incubation with 1.0 μ M OM significantly increased force development in the PKA-treated WT and SA myocardial preparations.

Discussion

Dysregulation of β -adrenergic signaling pathways in the pathological progression of HF leads to dephosphorylation of important regulatory myofilament proteins such as cMyBPC (El-Armouche et al., 2007; Jacques et al., 2008; Copeland et al., 2010; Kooij et al., 2013). While the phosphorylation of serine residues in cMyBPC's M domain is known to be a primary regulator of cardiac contractile function, the dependence of OM on variable cMyBPC phosphorylation has not been thoroughly investigated. Here we show that the basal cMyBPC dephosphorylation, often seen in advanced HF, blunts OM's inotropic influences on cardiac muscle contractility. We further show that OM attenuates the accelerating effects of cMyBPC PKA phosphorylation on XB kinetics.

cMyBPC dephosphorylation alters the myocardial contractile response to OM

Incubating WT and SA myocardial preparations with OM demonstrated a strong relationship between cMyBPC phosphorylation and the OM-induced contractile response. The effect of OM on the steady-state force generation parameters in the WT myocardial preparations with physiological baseline cMyBPC phosphorylation confirms results from previous studies (Mamidi et al., 2015). OM-dependent force enhancements in fibers were most dramatic at low Ca²⁺ concentrations (Table 2 and Fig. 3), as demonstrated previously (Mamidi et al., 2015, 2017b). Several lines of research indicate that OM accomplishes this effect by stabilizing the force-generating state of the XB cycle, leading to a prolonged duty ratio and increased cooperative activation of thin-filament regulatory units via nearestneighbor effects (Wang et al., 2014; Swenson et al., 2017; Gordon et al., 2000; Mamidi et al., 2015; Kampourakis et al., 2018). Furthermore, increasing the concentration of OM led to a dose-dependent increase in the force developed by the WT myocardial preparations (Table 2 and Fig. 3). OM's induction of Ca²⁺-independent activation mechanisms at low pCa also explains why OM increases pCa₅₀ and decreases force-pCa cooperativity (Table 3 and Fig. 5). With increasing Ca²⁺ concentrations, however, force enhancements become less pronounced (Table 2 and Fig. 3) as the effect of widespread Ca²⁺ activation overpowers the OM-induced cooperative XB activation (Mamidi et al., 2015, 2017b).

Also consistent with previous studies, OM substantially altered the dynamic XB behavior in the WT myocardial

preparations (Mamidi et al., 2015, 2017b). Increasing doses of OM progressively enhanced the immediate force response (P1) to a small rapid stretch in ML, reflecting a dose-dependent increase in XB stiffness in addition to an increased number of bound XBs at the time of stretch (Table 5 and Fig. 8 E). Nevertheless, OM decreased the final net magnitude of newly recruited XBs due to stretch activation (Pdf: Table 5 and Fig. 8 G). This effect may be due to an OM-induced reduction of the available XBs for recruitment following stretch activation. OM also slowed both $k_{\rm rel}$ and $k_{\rm df}$ in the myocardial preparations (Table 5 and Fig. 8). Several OM-mediated mechanisms may contribute to the slower $k_{\rm rel}$ including increasing the XB duty ratio, increasing XB stiffness (Mamidi et al., 2015), and slowing the myosin power stroke (Rohde et al., 2017; Caremani et al., 2019). The slowing in $k_{\rm df}$ may reflect the slow propagation in the rate of OM-induced cooperative thin-filament activation to adjacent regulatory units (Campbell, 1997; Mamidi et al., 2017b).

The phosphoablative cMyBPC mutations in the SA myocardial preparations significantly altered the contractile response to OM. While OM-mediated increases in force development were observed in the WT at low pCa (6.2 and 6.1), the SA myocardial preparations showed no significant force increases with 0.5 µM OM incubation (Table 2). No significant differences in pre-OM force generation and myofilament Ca²⁺ sensitivity (pCa₅₀) were observed between WT and SA myocardial preparations (Table 1 and Table 3). Following incubation with 1.0 µM OM, modest increases in forces were observed in the SA myocardial preparations, but the observed force increases were less dramatic than those observed in the corresponding WT myocardial preparations (Table 2). For example, the percent force increases following 1.0 µM OM incubation at pCa 6.2 and 6.1 in WT myocardial preparations were 157% and 63%, respectively, whereas percent force increases in SA myocardial preparations were only 51% and 33%, respectively (Table 2). Further deviating from the WT myocardial preparations, increasing OM concentration from 0.5 μ M to 1.0 μ M failed to significantly increase P1 in the SA myocardial preparations (Table 5, Fig. 6 B, and Fig. 8 F). These results suggest that cMyBPC dephosphorylation prevents OM from recruiting an equivalent number of XBs compared with basally phosphorylated WT cMyBPC. In this context, recent studies show that dephosphorylation of cMyBPC stabilizes a super-relaxed (SRX) state of myosin, which is characterized by very slow ATP turnover rates (McNamara



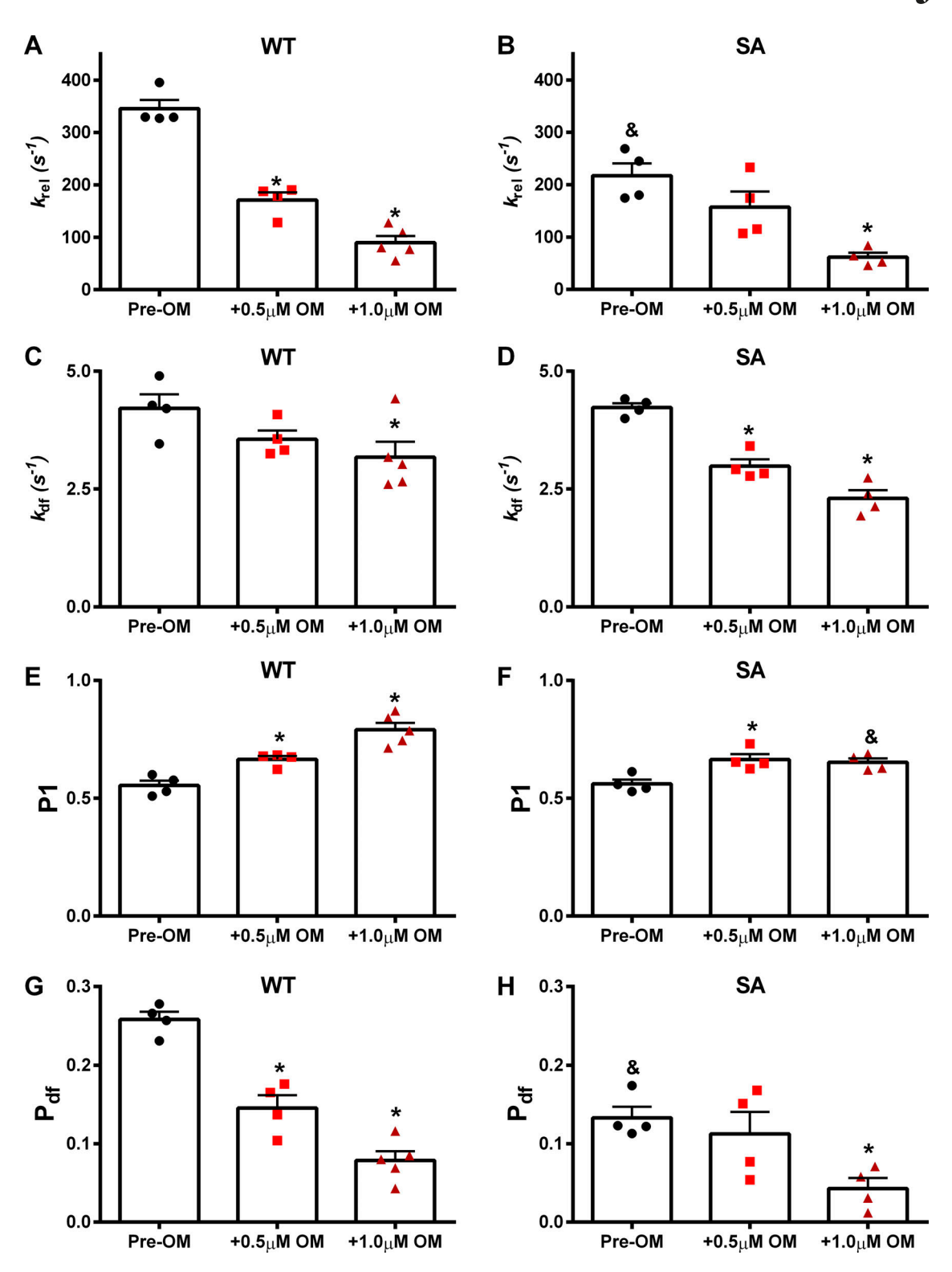


Figure 8. Impact of OM on the dynamic XB parameters in WT and SA myocardial preparations. The effects of OM on dynamic XB parameters derived from stretch activation responses in pre-OM, $0.5 \mu M$ OM-, and $1.0 \mu M$ -treated WT and SA myocardial preparations are shown at pCa 6.1. (A and B) k_{rel} before and following OM incubations in WT (A) and SA (B) myocardial preparations. (C and D) k_{df} before and following OM incubations in WT (C) and SA (D) myocardial preparations. (E and F) P1 before and following OM incubations in WT (E) and SA (F) myocardial preparations. (G and H) P_{df} before and following OM incubations in WT (G) and SA (H) myocardial preparations. Data from multiple preparations from each heart were averaged, and 12-15 myocardial preparations from four or five different hearts were used per group. Values are expressed as mean \pm SEM. *, Significantly different compared with the corresponding pre-OM group; P < 0.05. &, Significantly different compared with the corresponding WT group.



Table 6. Dynamic stretch activation parameters measured in PKA-treated WT and SA myocardial preparations

Group	k _{rel} (s ⁻¹)	k _{df} (s ⁻¹)	P1	P2	Р3	$P_{ m df}$
WT + PKA						
Pre-OM	573.48 ± 79.14	7.68 ± 1.07	0.637 ± 0.03	-0.062 ± 0.09	0.312 ± 0.08	0.374 ± 0.04
1.0 μΜ ΟΜ	124.46 ± 18.61 (*, P = 0.03)	2.58 ± 0.33 (*, P = 0.02)	0.724 ± 0.02 (*, P = 0.04)	0.055 ± 0.03	0.211 ± 0.02	0.156 ± 0.02 (*, P = 0.01)
SA + PKA						
Pre-OM	211.27 ± 2.60 (&, P = 0.01)	3.41 ± 0.26 (&, P = 0.02)	0.563 ± 0.03	0.126 ± 0.02	0.238 ± 0.01	0.112 ± 0.03 (&, P = 0.005)
1.0 μΜ ΟΜ	98.97 ± 11.81 (*, P = 0.01)	1.62 ± 0.40 (*, P = 0.01)	0.612 ± 0.02 (*, P = 0.02; &, P = 0.03)	0.156 ± 0.01 (&, P = 0.03)	0.212 ± 0.01	0.056 ± 0.01 (&, P = 0.01)

Stretch activation amplitudes were normalized to prestretch steady-state Ca^{2+} -activated force, which refers to the activation level (pCa 6.0; ~30% of maximal Ca^{2+} -activated force) as described in Materials and methods. k_{dfr} rate of XB recruitment; k_{relr} rate of XB detachment; P1, XB stiffness; P2, magnitude of XB detachment; P3, new steady-state force reached following a quick 2% stretch in ML; P_{dfr} magnitude of XB recruitment. Data from multiple preparations from each heart were averaged, and six to seven myocardial preparations from three different hearts were used per group. Values are expressed as mean \pm SEM. *, Significantly different compared to the corresponding pre-OM group. &, Significantly different compared with the corresponding WT group.

et al., 2019, 2015). Myosin heads in the SRX state are hypothesized to fold back toward the thick-filament backbone, and are unable to participate in active XB cycling (Woodhead et al., 2005; Spudich, 2019). Thus, it is likely that the phosphoablated cMyBPC present in SA myocardium would sequester more myosin heads to the SRX state, effectively removing them from the cycling XB population that OM can recruit to the force-generating state.

The myosin-sequestering effects of cMyBPC dephosphorylation can further explain the differences in $k_{\rm rel}$ seen between the OM-treated WT and SA myocardial preparations. In agreement with our previous studies (Mamidi et al., 2016, 2017a), we show that cMyBPC phosphoablation led to a slower pre-OM $k_{\rm rel}$ in SA when compared with WT myocardial preparations (Table 5). Additionally, we observed that the OM-mediated slowing effects on $k_{\rm rel}$ were more pronounced in the WT compared with the SA myocardial preparations, which required higher OM concentrations to achieve differences from baseline $k_{\rm rel}$, a likely effect of cMyBPC phosphoablation in the SA myocardial preparations (Table 5 and Fig. 8 B). Interestingly, k_{rel} in both groups converged to similar values at both 0.5 μM and 1.0 μM OM incubations (Table 5 and Fig. 8, A and B). By having fewer cycling XBs in the SA myocardial preparations at baseline, k_{rel} begins at a reduced value and OM has a diminished ability to slow k_{rel} further. Furthermore, a slowing in k_{rel} due to increasing OM concentrations also led to a decrease in the magnitude of XB detachment following a stretch in ML, leading to increase in P2 values which in turn contributed to the observed decreases in P_{df} (Table 5). In contrast to WT, the SA myocardial preparations showed an increasing trend in the P2 values following increased OM concentrations, but the P2 values post OM treatment did not reach a statistical significance when compared with P2 values of pre-OM SA myocardial preparations, indicating a differential effect of OM on P2 in a cMyBPC phosphoablated myocardium. Collectively, our findings suggest that cMyBPC dephosphorylation blunts OM-mediated force generation and alters the OMmediated XB behavior.

OM uncouples the sarcomere from β -adrenergic stimulation

To study the effects of OM on muscle contractile function in the context of β -adrenergic stimulation, we performed the 1.0 μ M OM experiments following incubation of the myocardial preparations with PKA. Numerous studies have established that cMyBPC phosphorylation is critical for an adequate cardiac response to β -adrenergic stimulation (Colson et al., 2010, 2012; Stelzer et al., 2006c; Tong et al., 2008; Gresham and Stelzer, 2016). Mechanistic models of cMyBPC phosphorylation suggest that the addition of negatively charged phosphates to M domain serine residues inhibits cMyBPC interactions with the S2 domain of myosin (Gautel et al., 1995; Spudich, 2019). Experimental evidence indicates that the loss of this interaction disrupts the SRX state of myosin heads (McNamara et al., 2019), increases myosin head proximity to the thin filament (Colson et al., 2008), and decreases XB stiffness (Stelzer et al., 2006c). These generally manifest as accelerated kinetics (increases in k_{rel} and k_{df} , Table 5 and Table 6) and an increased magnitude of XB detachment (Stelzer et al., 2006c). Our results show that OM incubation following cMyBPC phosphorylation by PKA largely counteracts these usual enhancements, resulting in increased XB stiffness, dramatically slowed kinetics, and decreases in the magnitude of XB detachment (Table 6). Most notably, OM slowed $k_{\rm rel}$ and $k_{\rm df}$ by ~78% and ~66%, respectively, in the PKA phosphorylated WT myocardial preparations following OM incubation (Table 6 and Fig. 9). The slowing effect of OM was so potent that neither $k_{\rm rel}$ nor $k_{\rm df}$ was statistically different from those measured in PKA and OM-treated SA myocardial preparations expressing the nonphosphorylatable cMyBPC (Table 6 and Fig. 9).

Strikingly, the effects of OM were largely the same regardless of whether the sarcomere was phosphorylated by PKA. One may have expected that the accelerating effects of cMyBPC phosphorylation would in some way cancel out the depressive effects of OM on XB behavior. However, we found that 1.0 μ M OM slowed XB detachment (k_{rel}) in both the PKA-treated and non-PKA WT muscle groups by similar amounts (~78% and ~73%,



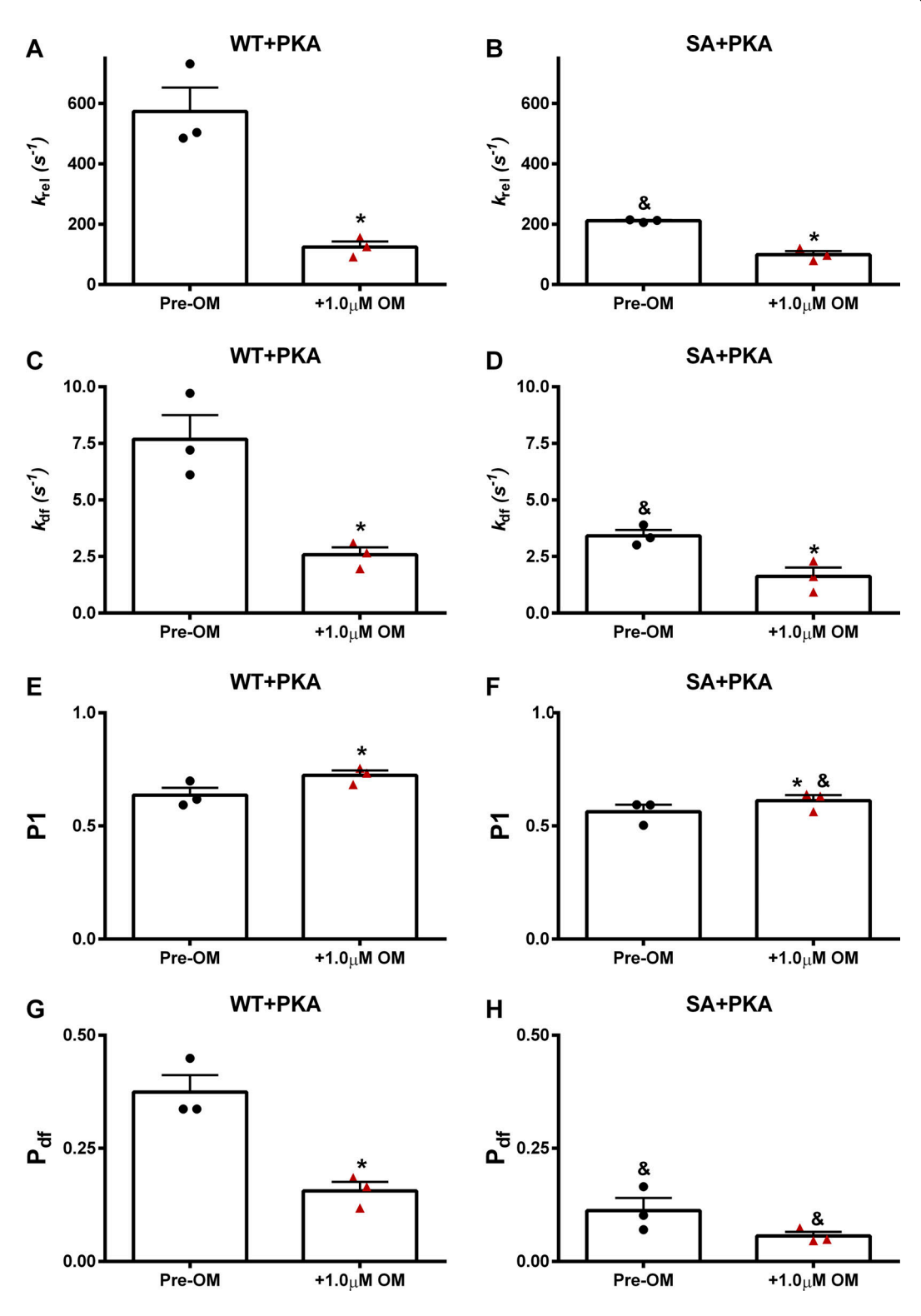


Figure 9. Impact of OM on the dynamic XB parameters in PKA-treated WT and SA myocardial preparations. The effects of OM on dynamic XB parameters derived from stretch activation responses in PKA-treated WT and SA myocardial preparations are shown at pCa 6.0. (A and B) k_{rel} before and following OM incubation in WT (A) and SA (B) myocardial preparations. (C and D) k_{df} before and following OM incubation in WT (C) and SA (D) myocardial preparations. (E and F) P1 before and following OM incubation in WT (E) and SA (F) myocardial preparations. (G and H) P_{df} before and following OM incubation in WT (G) and SA (H) myocardial preparations. Data from multiple preparations from each heart were averaged, and six to seven myocardial preparations from three different hearts were used per group. Values are expressed as mean \pm SEM. *, Significantly different compared with the corresponding pre-OM group; P < 0.05. &, Significantly different compared with the corresponding WT group.



respectively; Table 5, Table 6, Fig. 8, and Fig. 9). This would imply a mechanism where once myosin heads are freed from cMyBPC by its phosphorylation (McNamara et al., 2019), OM sequesters them to a slow cycling actin-bound state that cannot be accelerated by further PKA activity. Single-molecule studies have shown that OM creates such an actin-bound state by inhibiting the myosin power stroke, and trapping the XB in the prepower stroke position (Liu et al., 2015; Rohde et al., 2017). Our proposed mechanism would then assume that phosphorylated cMyBPC cannot accelerate the trapped XB through the power stroke, but we are unaware of studies that have investigated the effects of cMyBPC phosphorylation on the myosin power stroke. However, given that phosphorylated cMyBPC has lower affinity for myosin (Gautel et al., 1995), we find it unlikely that cMyBPC phosphorylation can accelerate the power stroke beyond that of cMyBPC-free myosin. This would suggest that the PKA phosphorylation of cMyBPC, and by extension the β-adrenergic pathway, is poorly positioned to counteract OMmediated kinetic slowing, because OM effectively uncouples myofilament contractility from β -adrenergic stimulation.

It is important to note that cMyBPC can modulate the sarcomere's contractile response by mechanisms not dependent on myosin binding. For instance, myosin-free cMyBPC N-terminal domains have been suggested to compete with myosin for actin binding sites and could therefore decrease the number of XBs that OM can recruit to the thin filament (Moss et al., 2015). This may explain why P_{df} remained significantly higher in the PKA-treated WT compared with the PKA-treated SA myocardial preparations following OM incubation and not in the non-PKA myocardial preparations (Table 5, Table 6, and Fig. 9). Nevertheless, the strong OM-dependent force increases and kinetic slowing we observed in the PKA-treated WT group suggest that effects due to cMyBPC actin binding are secondary to OM's potency (Table 6 and Fig. 9).

Clinical implications

Our finding that skinned myocardial preparations respond differently to OM concentration depending on the level of cMyBPC phosphorylation has important clinical implications for patients on OM therapy. Because β -adrenergic signaling dysregulation accompanies HF progression, PKA-mediated β -adrenergic phosphorylation of cMyBPC M domain residues decreases to low levels as patients progress toward end-stage HF (El-Armouche et al., 2007; Lohse et al., 2003; van der Velden and Stienen, 2019). Our results suggest that the therapeutic headroom of OM may be limited by intense cMyBPC dephosphorylation seen in advanced HF. Our observation could help explain why SV in HFrEF patients plateaus at OM plasma concentrations >400 ng/ml compared with healthy participants who continued to see increases with higher OM concentrations (Cleland et al., 2011; Teerlink et al., 2011).

Furthermore, short-term changes in β -adrenergic stimulation and cMyBPC phosphorylation due to physiological stressors like exercise could also modulate OM effects (Wang and Fitts, 2020; Leosco et al., 2007). While the β -adrenergic response to these stressors in end-stage HFrEF patients may not be dramatic, those in earlier stages of HF may still see a significant signaling

response (Leosco et al., 2007; Lohse et al., 2003). This healthier patient group is important to consider, as some researchers have postulated that OM should be administered to early-stage HF patients to maximize its potential reverse-remodeling effects (Ahmad et al., 2019). Our data from PKA-treated myocardial preparations suggests that OM stifles normal β-adrenergic-mediated contractile acceleration and could blunt the cardiac response needed to accommodate normal physiological stressors resulting in ischemia. Ischemia has been observed in patients taking high doses of OM at rest, but increased cardiac demand could worsen this risk even at lower OM doses (Teerlink et al., 2011; Cleland et al., 2011; Nánási et al., 2016; Rønning et al., 2018). At this time, however, clinical trials studying the safety of OM in the context of exercise have focused only on end-stage HFrEF patients with baseline ischemia under nonstrenuous exercise (Greenberg et al., 2015). Taken together, results from this study demonstrate the importance of accounting for basal cMyBPC phosphorylation levels and the interplay between OM and the myofilament contractile regulation in HF therapies.

Acknowledgments

Henk L. Granzier served as editor.

All experiments were performed at the Department of Physiology and Biophysics, Case Western Reserve University, Cleveland, OH.

This work was supported by the National Institutes of Health (grants R01 HL146676 and HL-114770).

The authors declare no competing financial interests.

Author contributions: R. Mamidi, J.B. Holmes, and J.E. Stelzer contributed to the conception and design of the experiments. R. Mamidi, J.B. Holmes, C.Y. Doh, K.L. Dominic, N. Madugula, and J.E. Stelzer participated in performing the experiments, data collection, analysis, data interpretation, writing, and revising the manuscript. All authors approved the final version of the manuscript.

Submitted: 2 November 2020 Accepted: 27 January 2021

References

Ahmad, T., P.E. Miller, M. McCullough, N.R. Desai, R. Riello, M. Psotka, M. Böhm, L.A. Allen, J.R. Teerlink, G.M.C. Rosano, and J. Lindenfeld. 2019. Why has positive inotropy failed in chronic heart failure? Lessons from prior inotrope trials. Eur. J. Heart Fail. 21:1064–1078. https://doi.org/10.1002/ejhf.1557

Bardswell, S.C., F. Cuello, J.C. Kentish, and M. Avkiran. 2012. cMyBP-C as a promiscuous substrate: phosphorylation by non-PKA kinases and its potential significance. J. Muscle Res. Cell Motil. 33:53-60. https://doi.org/ 10.1007/s10974-011-9276-3

Campbell, K. 1997. Rate constant of muscle force redevelopment reflects cooperative activation as well as cross-bridge kinetics. *Biophys. J.* 72: 254–262. https://doi.org/10.1016/S0006-3495(97)78664-8

Campbell, K.S., and R.L. Moss. 2003. SLControl: PC-based data acquisition and analysis for muscle mechanics. Am. J. Physiol. Heart Circ. Physiol. 285:H2857-H2864. https://doi.org/10.1152/ajpheart.00295.2003

Candiano, G., M. Bruschi, L. Musante, L. Santucci, G.M. Ghiggeri, B. Carnemolla, P. Orecchia, L. Zardi, and P.G. Righetti. 2004. Blue silver: a very sensitive colloidal Coomassie G-250 staining for proteome analysis. Electrophoresis. 25:1327-1333. https://doi.org/10.1002/elps.200305844



- Caremani, M., F. Pinzauti, J.D. Powers, S. Governali, T. Narayanan, G.J.M. Stienen, M. Reconditi, M. Linari, V. Lombardi, and G. Piazzesi. 2019. Inotropic interventions do not change the resting state of myosin motors during cardiac diastole. J. Gen. Physiol. 151:53–65. https://doi.org/10.1085/jgp.201812196
- Chandra, M., R. Mamidi, S. Ford, C. Hidalgo, C. Witt, C. Ottenheijm, S. Labeit, and H. Granzier. 2009. Nebulin alters cross-bridge cycling kinetics and increases thin filament activation: a novel mechanism for increasing tension and reducing tension cost. *J. Biol. Chem.* 284:30889–30896. https://doi.org/10.1074/jbc.M109.049718
- Cleland, J.G.F., J.R. Teerlink, R. Senior, E.M. Nifontov, J.J. Mc Murray, C.C. Lang, V.A. Tsyrlin, B.H. Greenberg, J. Mayet, D.P. Francis, et al. 2011. The effects of the cardiac myosin activator, omecamtiv mecarbil, on cardiac function in systolic heart failure: a double-blind, placebo-controlled, crossover, dose-ranging phase 2 trial. *Lancet.* 378:676–683. https://doi.org/10.1016/S0140-6736(11)61126-4
- Colson, B.A., T. Bekyarova, M.R. Locher, D.P. Fitzsimons, T.C. Irving, and R.L. Moss. 2008. Protein kinase A-mediated phosphorylation of cMyBP-C increases proximity of myosin heads to actin in resting myocardium. Circ. Res. 103:244–251. https://doi.org/10.1161/CIRCRESAHA.108.178996
- Colson, B.A., M.R. Locher, T. Bekyarova, J.R. Patel, D.P. Fitzsimons, T.C. Irving, and R.L. Moss. 2010. Differential roles of regulatory light chain and myosin binding protein-C phosphorylations in the modulation of cardiac force development. J. Physiol. 588:981-993. https://doi.org/10.1113/jphysiol.2009.183897
- Colson, B.A., J.R. Patel, P.P. Chen, T. Bekyarova, M.I. Abdalla, C.W. Tong, D.P. Fitzsimons, T.C. Irving, and R.L. Moss. 2012. Myosin binding protein-C phosphorylation is the principal mediator of protein kinase A effects on thick filament structure in myocardium. *J. Mol. Cell. Cardiol.* 53:609–616. https://doi.org/10.1016/j.yjmcc.2012.07.012
- Copeland, O., S. Sadayappan, A.E. Messer, G.J.M. Steinen, J. van der Velden, and S.B. Marston. 2010. Analysis of cardiac myosin binding protein-C phosphorylation in human heart muscle. J. Mol. Cell. Cardiol. 49: 1003–1011. https://doi.org/10.1016/j.yjmcc.2010.09.007
- Coulton, A.T., and J.E. Stelzer. 2012. Cardiac myosin binding protein C and its phosphorylation regulate multiple steps in the cross-bridge cycle of muscle contraction. *Biochemistry*. 51:3292–3301. https://doi.org/10.1021/bi300085x
- Craig, R., K.H. Lee, J.Y. Mun, I. Torre, and P.K. Luther. 2014. Structure, sarcomeric organization, and thin filament binding of cardiac myosin-binding protein-C. *Pflugers Arch.* 466:425–431. https://doi.org/10.1007/s00424-013-1426-6
- Doh, C.Y., J. Li, R. Mamidi, and J.E. Stelzer. 2019. The HCM-causing Y235S cMyBPC mutation accelerates contractile function by altering C1 domain structure. Biochim. Biophys. Acta Mol. Basis Dis. 1865:661-677. https://doi.org/10.1016/j.bbadis.2019.01.007
- El-Armouche, A., L. Pohlmann, S. Schlossarek, J. Starbatty, Y.H. Yeh, S. Nattel, D. Dobrev, T. Eschenhagen, and L. Carrier. 2007. Decreased phosphorylation levels of cardiac myosin-binding protein-C in human and experimental heart failure. J. Mol. Cell. Cardiol. 43:223–229. https://doi.org/10.1016/j.yjmcc.2007.05.003
- Fabiato, A. 1988. Computer programs for calculating total from specified free or free from specified total ionic concentrations in aqueous solutions containing multiple metals and ligands. *Methods Enzymol.* 157:378–417. https://doi.org/10.1016/0076-6879(88)57093-3
- Ford, S.J., M. Chandra, R. Mamidi, W. Dong, and K.B. Campbell. 2010. Model representation of the nonlinear step response in cardiac muscle. J. Gen. Physiol. 136:159–177. https://doi.org/10.1085/jgp.201010467
- Gautel, M., O. Zuffardi, A. Freiburg, and S. Labeit. 1995. Phosphorylation switches specific for the cardiac isoform of myosin binding protein-C: a modulator of cardiac contraction? EMBO J. 14:1952–1960. https://doi.org/10.1002/j.1460-2075.1995.tb07187.x
- Godt, R.E., and B.D. Lindley. 1982. Influence of temperature upon contractile activation and isometric force production in mechanically skinned muscle fibers of the frog. J. Gen. Physiol. 80:279–297. https://doi.org/10 .1085/jgp.80.2.279
- Gollapudi, S.K., S.M. Reda, and M. Chandra. 2017. Omecamtiv Mecarbil Abolishes Length-Mediated Increase in Guinea Pig Cardiac Myofiber Ca²⁺ Sensitivity. Biophys. J. 113:880–888. https://doi.org/10.1016/j.bpj .2017.07.002
- Gordon, A.M., E. Homsher, and M. Regnier. 2000. Regulation of contraction in striated muscle. *Physiol. Rev.* 80:853–924. https://doi.org/10.1152/ physrev.2000.80.2.853
- Greenberg, B.H., W. Chou, K.G. Saikali, R. Escandón, J.H. Lee, M.M. Chen, T. Treshkur, I. Megreladze, S.M. Wasserman, P. Eisenberg, et al. 2015.

- Safety and tolerability of omecamtiv mecarbil during exercise in patients with ischemic cardiomyopathy and angina. *JACC Heart Fail.* 3: 22–29. https://doi.org/10.1016/j.jchf.2014.07.009
- Gresham, K.S., R. Mamidi, and J.E. Stelzer. 2014. The contribution of cardiac myosin binding protein-c Ser282 phosphorylation to the rate of force generation and in vivo cardiac contractility. J. Physiol. 592:3747–3765. https://doi.org/10.1113/jphysiol.2014.276022
- Gresham, K.S., and J.E. Stelzer. 2016. The contributions of cardiac myosin binding protein C and troponin I phosphorylation to β-adrenergic enhancement of in vivo cardiac function. *J. Physiol.* 594:669–686. https://doi.org/10.1113/IP270959
- Gruen, M., and M. Gautel. 1999. Mutations in β-myosin S2 that cause familial hypertrophic cardiomyopathy (FHC) abolish the interaction with the regulatory domain of myosin-binding protein-C. *J. Mol. Biol.* 286: 933–949. https://doi.org/10.1006/jmbi.1998.2522
- Holmes, J.B., C.Y. Doh, R. Mamidi, J. Li, and J.E. Stelzer. 2020. Strategies for targeting the cardiac sarcomere: avenues for novel drug discovery. Expert Opin. Drug Discov. 15:457–469. https://doi.org/10.1080/17460441 .2020.1722637
- Jacques, A.M., O. Copeland, A.E. Messer, C.E. Gallon, K. King, W.J. McKenna, V.T. Tsang, and S.B. Marston. 2008. Myosin binding protein C phosphorylation in normal, hypertrophic and failing human heart muscle. *J. Mol. Cell. Cardiol.* 45:209–216. https://doi.org/10.1016/j.yjmcc.2008.05.020
- Kampourakis, T., X. Zhang, Y.-B.B. Sun, and M. Irving. 2018. Omecamtiv mercabil and blebbistatin modulate cardiac contractility by perturbing the regulatory state of the myosin filament. J. Physiol. 596:31-46. https://doi.org/10.1113/JP275050
- Kooij, V., R.J. Holewinski, A.M. Murphy, and J.E. Van Eyk. 2013. Characterization of the cardiac myosin binding protein-C phosphoproteome in healthy and failing human hearts. J. Mol. Cell. Cardiol. 60:116–120. https://doi.org/10.1016/j.yjmcc.2013.04.012
- Leosco, D., G. Rengo, G. Iaccarino, A. Filippelli, A. Lymperopoulos, C. Zincarelli, F. Fortunato, L. Golino, M. Marchese, G. Esposito, et al. 2007. Exercise training and β-blocker treatment ameliorate age-dependent impairment of β-adrenergic receptor signaling and enhance cardiac responsiveness to adrenergic stimulation. Am. J. Physiol. Heart Circ. Physiol. 293:H1596-H1603. https://doi.org/10.1152/ajpheart.00308.2007
- Li, J., K.S. Gresham, R. Mamidi, C.Y. Doh, X. Wan, I. Deschenes, and J.E. Stelzer. 2018. Sarcomere-based genetic enhancement of systolic cardiac function in a murine model of dilated cardiomyopathy. *Int. J. Cardiol.* 273:168–176. https://doi.org/10.1016/j.ijcard.2018.09.073
- Li, J., R. Mamidi, C.Y. Doh, J.B. Holmes, N. Bharambe, R. Ramachandran, and J.E. Stelzer. 2020. AAV9 gene transfer of cMyBPC N-terminal domains ameliorates cardiomyopathy in cMyBPC-deficient mice. *JCI Insight*. 5: e130182. https://doi.org/10.1172/jci.insight.130182
- Liu, Y., H.D. White, B. Belknap, D.A. Winkelmann, and E. Forgacs. 2015. Omecamtiv Mecarbil modulates the kinetic and motile properties of porcine β-cardiac myosin. Biochemistry. 54:1963–1975. https://doi.org/10.1021/bi5015166
- Lohse, M.J., S. Engelhardt, and T. Eschenhagen. 2003. What is the role of β-adrenergic signaling in heart failure? Circ. Res. 93:896-906. https:// doi.org/10.1161/01.RES.0000102042.83024.CA
- Malik, F.I., J.J. Hartman, K.A. Elias, B.P. Morgan, H. Rodriguez, K. Brejc, R.L. Anderson, S.H. Sueoka, K.H. Lee, J.T. Finer, et al. 2011. Cardiac Myosin Activation: A Potential Therapeutic Approach for Systolic Heart Failure. Science. 331:1439–1443. https://doi.org/10.1126/science.1200113
- Mamidi, R., K.S. Gresham, and J.E. Stelzer. 2014. Length-dependent changes in contractile dynamics are blunted due to cardiac myosin binding protein-C ablation. Front. Physiol. 5:461. https://doi.org/10.3389/fphys .2014.00461
- Mamidi, R., K.S. Gresham, A. Li, C.G. dos Remedios, and J.E. Stelzer. 2015. Molecular effects of the myosin activator omecamtiv mecarbil on contractile properties of skinned myocardium lacking cardiac myosin binding protein-C. J. Mol. Cell. Cardiol. 85:262–272. https://doi.org/10 .1016/j.yjmcc.2015.06.011
- Mamidi, R., K.S. Gresham, S. Verma, and J.E. Stelzer. 2016. Cardiac myosin binding protein-C phosphorylation modulates myofilament lengthdependent activation. Front. Physiol. 7:38. https://doi.org/10.3389/ fphys.2016.00038
- Mamidi, R., K.S. Gresham, J. Li, and J.E. Stelzer. 2017a. Cardiac myosin binding protein-C Ser³⁰² phosphorylation regulates cardiac β-adrenergic reserve. Sci. Adv. 3:e1602445. https://doi.org/10.1126/sciadv .1602445
- Mamidi, R., J. Li, K.S. Gresham, S. Verma, C.Y. Doh, A. Li, S. Lal, C.G. Dos Remedios, and J.E. Stelzer. 2017b. Dose-Dependent Effects of the Myosin



- Activator Omecamtiv Mecarbil on Cross-Bridge Behavior and Force Generation in Failing Human Myocardium. *Circ. Heart Fail.* 10:e004257. https://doi.org/10.1161/CIRCHEARTFAILURE.117.004257
- Mamidi, R., J. Li, C.Y. Doh, S. Verma, and J.E. Stelzer. 2018. Impact of the Myosin Modulator Mavacamten on Force Generation and Cross-Bridge Behavior in a Murine Model of Hypercontractility. J. Am. Heart Assoc. 7: e009627. https://doi.org/10.1161/JAHA.118.009627
- Mamidi, R., J. Li, C.Y. Doh, J.B. Holmes, and J.E. Stelzer. 2019. Lost in translation: Interpreting cardiac muscle mechanics data in clinical practice. Arch. Biochem. Biophys. 662:213–218. https://doi.org/10.1016/j.abb.2018.12.021
- McNamara, J.W., A. Li, C.G. Dos Remedios, and R. Cooke. 2015. The role of super-relaxed myosin in skeletal and cardiac muscle. *Biophys. Rev.* 7: 5–14. https://doi.org/10.1007/s12551-014-0151-5
- McNamara, J.W., R.R. Singh, and S. Sadayappan. 2019. Cardiac myosin binding protein-C phosphorylation regulates the super-relaxed state of myosin. Proc. Natl. Acad. Sci. USA. 116:11731–11736. https://doi.org/10 .1073/pnas.1821660116
- Moss, R.L., D.P. Fitzsimons, and J.C. Ralphe. 2015. Cardiac MyBP-C regulates the rate and force of contraction in mammalian myocardium. *Circ. Res.* 116:183–192. https://doi.org/10.1161/CIRCRESAHA.116.300561
- Nagayama, T., E. Takimoto, S. Sadayappan, J.O. Mudd, J.G. Seidman, J. Robbins, and D.A. Kass. 2007. Control of in vivo contraction/relaxation kinetics by myosin binding protein C: Protein kinase A phosphorylation-dependent and -independent regulation. *Circulation*. 116:2399–2408. https://doi.org/10.1161/CIRCULATIONAHA.107.706523
- Nánási, P. Jr., K. Váczi, and Z. Papp. 2016. The myosin activator omecamtiv mecarbil: a promising new inotropic agent. Can. J. Physiol. Pharmacol. 94:1033-1039. https://doi.org/10.1139/cjpp-2015-0573
- Psotka, M.A., S.S. Gottlieb, G.S. Francis, L.A. Allen, J.R. Teerlink, K.F. Adams Jr., G.M.C. Rosano, and P. Lancellotti. 2019. Cardiac Calcitropes, Myotropes, and Mitotropes: JACC Review Topic of the Week. J. Am. Coll. Cardiol. 73:2345–2353. https://doi.org/10.1016/j.jacc.2019.02.051
- Rohde, J.A., D.D. Thomas, and J.M. Muretta. 2017. Heart failure drug changes the mechanoenzymology of the cardiac myosin powerstroke. *Proc. Natl. Acad. Sci. USA*. 114:E1796–E1804. https://doi.org/10.1073/pnas.1611698114
- Rønning, L., J.P. Bakkehaug, L. Rødland, A.B. Kildal, T. Myrmel, and O.-J. How. 2018. Opposite diastolic effects of omecamtiv mecarbil versus dobutamine and ivabradine co-treatment in pigs with acute ischemic heart failure. Physiol. Rep. 6:e13879. https://doi.org/10.14814/phy2.13879
- Rosas, P.C., Y. Liu, M.I. Abdalla, C.M. Thomas, D.T. Kidwell, G.F. Dusio, D. Mukhopadhyay, R. Kumar, K.M. Baker, B.M. Mitchell, et al. 2015. Phosphorylation of cardiac Myosin-binding protein-C is a critical mediator of diastolic function. Circ. Heart Fail. 8:582–594. https://doi.org/10.1161/CIRCHEARTFAILURE.114.001550
- Shen, Y.-T., F.I. Malik, X. Zhao, C. Depre, S.K. Dhar, P. Abarzúa, D.J. Morgans, and S.F. Vatner. 2010. Improvement of cardiac function by a cardiac Myosin activator in conscious dogs with systolic heart failure. Circ. Heart Fail. 3:522–527. https://doi.org/10.1161/CIRCHEARTFAILURE.109.930321
- Spudich, J.A. 2019. Three perspectives on the molecular basis of hyper-contractility caused by hypertrophic cardiomyopathy mutations. Pflugers Arch. 471:701–717. https://doi.org/10.1007/s00424-019-02259-2
- Stelzer, J.E., and R.L. Moss. 2006. Contributions of stretch activation to length-dependent contraction in murine myocardium. J. Gen. Physiol. 128:461-471. https://doi.org/10.1085/jgp.200609634
- Stelzer, J.E., D.P. Fitzsimons, and R.L. Moss. 2006a. Ablation of myosinbinding protein-C accelerates force development in mouse

- myocardium. *Biophys. J.* 90:4119–4127. https://doi.org/10.1529/biophysj.105.078147
- Stelzer, J.E., L. Larsson, D.P. Fitzsimons, and R.L. Moss. 2006b. Activation dependence of stretch activation in mouse skinned myocardium: implications for ventricular function. J. Gen. Physiol. 127:95–107. https://doi .org/10.1085/jgp.200509432
- Stelzer, J.E., J.R. Patel, and R.L. Moss. 2006c. Protein kinase A-mediated acceleration of the stretch activation response in murine skinned myocardium is eliminated by ablation of cMyBP-C. Circ. Res. 99:884–890. https://doi.org/10.1161/01.RES.0000245191.34690.66
- Stelzer, J.E., J.R. Patel, J.W. Walker, and R.L. Moss. 2007. Differential roles of cardiac myosin-binding protein C and cardiac troponin I in the myofibrillar force responses to protein kinase A phosphorylation. Circ. Res. 101:503-511. https://doi.org/10.1161/CIRCRESAHA.107.153650
- Swenson, A.M., W. Tang, C.A. Blair, C.M. Fetrow, W.C. Unrath, M.J. Previs, K.S. Campbell, C.M. Yengo. 2017. Omecamtiv mecarbil enhances the duty ratio of human β-cardiac myosin resulting in increased calcium sensitivity and slowed force development in cardiac muscle. J. Biol. Chem. 292:3768–3778. https://doi.org/10.1074/jbc.M116.748780
- Takahashi, R., M.A.H. Talukder, and M. Endoh. 2000. Inotropic effects of OR-1896, an active metabolite of levosimendan, on canine ventricular myocardium. Eur. J. Pharmacol. 400:103–112. https://doi.org/10.1016/ S0014-2999(00)00385-X
- Teerlink, J.R., C.P. Clarke, K.G. Saikali, J.H. Lee, M.M. Chen, R.D. Escandon, L. Elliott, R. Bee, M.R. Habibzadeh, J.H. Goldman, et al. 2011. Dose-dependent augmentation of cardiac systolic function with the selective cardiac myosin activator, omecamtiv mecarbil: a first-in-man study. Lancet. 378:667-675. https://doi.org/10.1016/S0140-6736(11) 61219-1
- Teerlink, J.R., R. Diaz, G.M. Felker, J.J.V. McMurray, M. Metra, S.D. Solomon, K.F. Adams, I. Anand, A. Arias-Mendoza, T. Biering-Sørensen, et al. 2020a. Omecamtiv mecarbil in chronic heart failure with reduced ejection fraction: GALACTIC-HF baseline characteristics and comparison with contemporary clinical trials. Eur. J. Heart Fail. 22:2160–2171. https://doi.org/10.1002/ejhf.2015
- Teerlink, J.R., R. Diaz, G.M. Felker, J.J.V. McMurray, M. Metra, S.D. Solomon, J.C. Legg, G. Büchele, C. Varin, C.E. Kurtz, et al. 2020b. Omecamtiv Mecarbil in Chronic Heart Failure With Reduced Ejection Fraction: Rationale and Design of GALACTIC-HF. JACC Heart Fail. 8:329–340. https://doi.org/10.1016/j.jchf.2019.12.001
- Tong, C.W., J.E. Stelzer, M.L. Greaser, P.A. Powers, and R.L. Moss. 2008. Acceleration of crossbridge kinetics by protein kinase A phosphorylation of cardiac myosin binding protein C modulates cardiac function. Circ. Res. 103:974–982. https://doi.org/10.1161/CIRCRESAHA.108.177683
- van der Velden, J., and G.J.M. Stienen. 2019. Cardiac Disorders and Pathophysiology of Sarcomeric Proteins. Physiol. Rev. 99:381–426. https://doi .org/10.1152/physrev.00040.2017
- Wang, X., and R.H. Fitts. 2020. Cardiomyocyte slowly activating delayed rectifier potassium channel: regulation by exercise and β-adrenergic signaling. *J Appl Physiol* (1985). 128:1177–1185. https://doi.org/10.1152/japplphysiol.00802.2019
- Wang, Y., K. Ajtai, and T.P. Burghardt. 2014. Analytical comparison of natural and pharmaceutical ventricular myosin activators. *Biochemistry*. 53: 5298–5306. https://doi.org/10.1021/bi500730t
- Woodhead, J.L., F.Q. Zhao, R. Craig, E.H. Egelman, L. Alamo, and R. Padrón. 2005. Atomic model of a myosin filament in the relaxed state. *Nature*. 436:1195–1199. https://doi.org/10.1038/nature03920